Last interglacial sea-level proxies in the Korean Peninsula

Woo Hun Ryang[1], Alexander R. Simms[2], Hyun Ho Yoon[3], Seung Soo Chun[4], and Gee Soo Kong[5]

[1] Division of Science Education and Institute of Science Education, Jeonbuk National University, Jeonju, Jeonbuk 54896, Republic of Korea

5   [2] Department of Earth Science, University of California, Santa Barbara, California 93106, U.S.A.

[3] Geological Research Division, Korea Institute of Geoscience and Mineral Resources (KIGAM), Daejeon 34132, Republic of Korea

[4] Faculty of Earth System & Environmental Sciences, Chonnam National University, Gwangju 61186, Republic of Korea

[5] Petroleum and Marine Research Division, Korea Institute of Geoscience and Mineral Resources (KIGAM), Daejeon 34132,
10   Republic of Korea

Correspondence to: Woo Hun Ryang (ryang@jbnu.ac.kr)

Abstract. Like most of the world's coastlines, the Korean Peninsula experienced higher-than-present sea levels during the Last Interglacial (LIG) otherwise known as Marine Isotope Stage (MIS) 5e. However, the expression of that highstand in the geological record differs across the eastern and western Korean Peninsula. The tectonically active east coast of the Korean
15   Peninsula is characterized by broad uplifted marine terraces, while the stable west coast is characterized by tidal flats and rias. In this study, we used a standardized database template to review and extract the existing constraints on LIG sea levels along both the east and west coasts of the Korean Peninsula. A total of 62 LIG constraining data points were compiled including 34 sea-level indicators, 22 marine limiting records, and 6 terrestrial limiting records. The ages from these data points are based on 61 optically stimulated luminescence (OSL) measurements and 1 paleomagnetic-based age. Along the uplifted east coast,
20   LIG sea-level indicators based on marine terraces are at elevations ranging from +9 to +32 m. The uplifted marine terraces are cut or otherwise deformed by faults developed under a compressional regime due to backarc closing of the East Sea since the early Pliocene. As a result, tectonic uplift likely has affected the elevations of the east coast LIG shorelines. In contrast, LIG sea-level records on the west coast of the Korean Peninsula are found at heights of between +3 and +6 m and include marine and terrestrial elevation-limiting records as well as true sea-level indicators. The LIG sea-level constraints along the west coast
25   of the Korean Peninsula are likely unaffected by vertical movement or experienced minor subsidence during the Quaternary.

1 Introduction

During the Last Interglacial (LIG), otherwise known as Marine Isotope Stage (MIS) 5e (about 130 to 115 ka), global sea level was 5~9 m higher than present sea level (Veeh, 1966; Dutton and Lambeck, 2012). However, the apparent magnitude of that highstand is expressed differently across the globe depending on local tectonics, glacial-isostatic adjustment (GIA) processes,
30   and sediment compaction. Due to their contrasting tectonic settings, the eastern and western coasts of the Korean Peninsula

record that global highstand in sea levels differently. The eastern Korean Peninsula is tectonically active while the western Korean Peninsula has been relatively stable throughout the Quaternary (Chough et al., 2000; Chough, 2013). As a result, the active east coast of the Korean Penisula is characterized by broad uplifted marine terraces (S.J. Choi, 2019; G.Y. Lee and Park, 2019b), while the more stable west coast hosts tidal environments of its ria coast (Chough et al., 2004; Cummings et al.,

35   2016). Available LIG constraints from the east coast are based primarily on raised beach deposits overlying marine terraces, while those of the west coast are based on both presently submerged and subaerial tidal deposits. Although marine terraces are more prominent with a higher potential of preserving coastal indicators reflecting higher sea levels (Shennan et al., 2015; Rovere et al., 2016), sea-level records based on tidal deposit along the west coast actually may provide more valuable MIS 5e sea-level records. The value of the sea level indicators of the western Korean Peninsula is in part due to relatively minor glacial

40   isostatic adjustment (GIA) effects across the Korean Peninsula (Creveling et al., 2017) and tectonic stability (Chough et al., 2000; Chough, 2013). In this paper, we summarize the two contrasting datasets of MIS5e relative sea-level (RSL) changes from the two different tectonic settings of the eastern and western Korean Peninsula.

This work is part of the World Atlas of Last Interglacial Shorelines (WALIS) whose aim is to construct a database of LIG RSL indicators from across the globe (https://warmcoasts.eu/world-atlas.html). This paper reviews the LIG sea-level

45   constraints from the Korean Peninsula entered into the online WALIS database (zenodo). A total of 75 papers including 68 published and 7 unpublished studies were reviewed to extract 62 LIG data points comprising 34 sea-level indicators, 22 marine limiting records, and 6 terrestrial limiting records. These data are based on 61 optically stimulated luminescence (OSL) ages and 1 paleomagnetic-constraint. The database for the Korean Peninsula is available open-access in spreadsheet format as Ryang and Simms (2021; https://doi.org/10.5281/zenodo.4974826). A description of the database fields is available from

50   Rovere et al. (2020; https://doi.org/10.5281/zenodo.3961543).

2 Background

2.1 Geological and Oceanographic overview

The tectonic framework of the Korean Peninsula reflects the large-scale interaction between the Pacific, Eurasian, and Indian plates during the Cenozoic. Two major tectonic processes govern that framework: northwestward subduction of the Pacific

55   Plate beneath the eastern margin of the Eurasia Plate and eastward extrusion of continental crust due to the India-Eurasia collision (Molnar and Tapponnier, 1975; Watson et al., 1987; Schellart and Lister, 2005).

The East Sea (Sea of Japan) is a backarc basin on the eastern margin of the Eurasia Plate, which opened and subsided during the early Oligocene through middle Miocene (32 to 10 Ma) (Fig. 1; Ingle, 1992; Tamaki et al., 1992; Chough et al., 2000). Since the early Pliocene (5 Ma), the region has experienced backarc closing resulting in compressional deformation (S.H.

60   Yoon and Chough, 1995; Kwon et al., 2009). The compressional deformation caused uplift of the eastern Korean continental margin throughout the Quaternary (Fig. 2; Chough et al., 2000). Uplift resulted in the development of Quaternary marine terraces along the eastern shoreline of the Korean Peninsula (Figs. 3 to 6). The marine terraces are grouped into 4 to 6 sets on

the basis of their elevation, ranging from 3 to 130 m above present sea level (S.W. Kim, 1973; Oh, 1977; D.Y. Lee, 1987). Individual terraces are overlain by 2-40 m of unconsolidated marine and aeolian sands and well-rounded beach gravels (Chough et al., 2000).
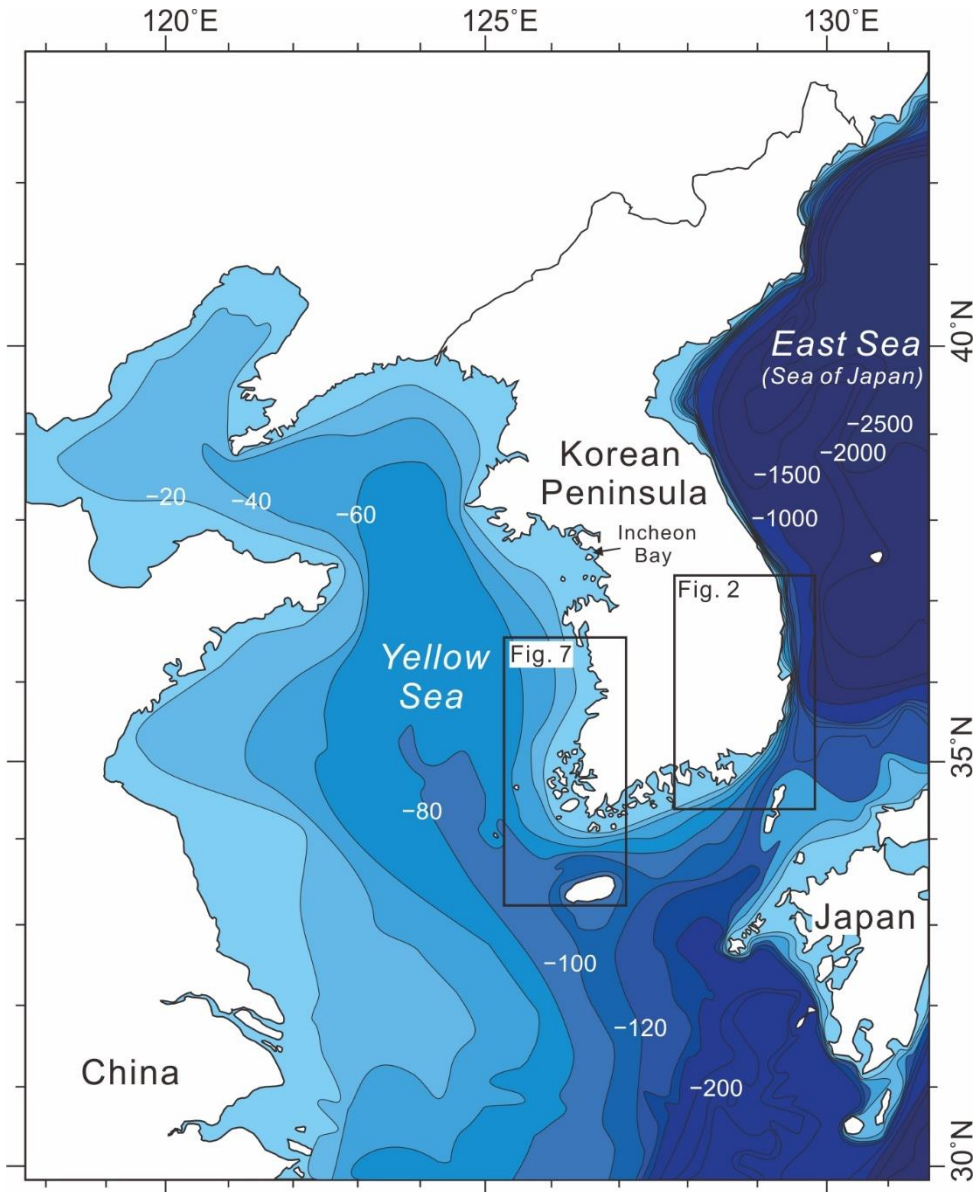
Figure 1: Bathymetry around the Korean Peninsula (modified after Chough et al., 2000; 2004; Cummings et al., 2016). Bathymetric contour inveral is in meters. Detailed maps with sampling areas are shown in Figs. 2, 7.
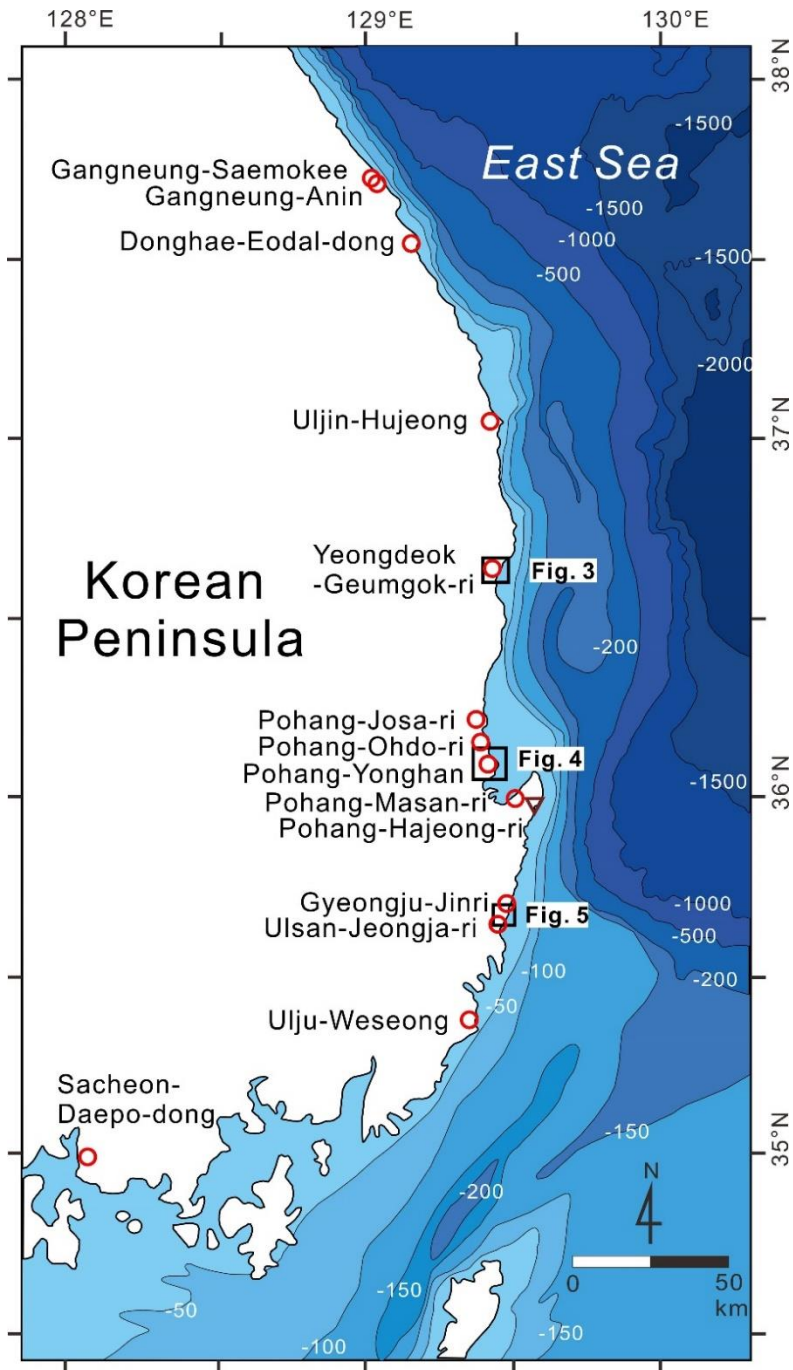
Figure 2: Map of the eastern and southern Korean Peninsula showing detailed bathymetry and marine terraces locations. Red circles represent sea-level indicator locations based on OSL ages with exception of the Pohang-Masan-ri area which has an additional paleomagnetic-based age. An inverted triangle shows the location of a terrestrial-limiting point. Age data can be found in Table 3. Bathymetric contour inveral is in meters.

The East Sea is a semi-enclosed marginal sea with an average water depth of about 1350 m and a maximum water depth of about 3700 m west of the Japanese Island of Hokkaido (Chough et al., 2000). The eastern continental shelf is narrow and rapidly transitions into a deep basin (Fig. 1). Along the east coast of Korea, the tides are microtidal ranging from 10 to 30 cm, based on tide-gauges around the coast and satellite altimeter-derived (TOPEX/Poseidon) sea-surface heights (Nam et al., 2004; 2015).

The Yellow Sea is a semi-enclosed shallow epicontinental sea with an average water depth of about 55 m and a maximum depth nearing 100 m at its southeastern margin (Fig. 1; Chough et al., 2000). The seafloor of the Yellow Sea is flat and broad (Fig. 1). Based on tide-gauge observations, the tides are semidiurnal, and the tidal range varies from mesotidal (2-4 m) along the open coast to macrotidal (>4 m) within embayments (Oh and Lee, 1998; Cummings et al., 2016). Presently, high-tide beaches, multiple swash bars, cheniers, and sandy tidal-flat deposits are found along the open coast, while mud-rich tidal deposits dominate the embayed coastlines (Figs. 7, 8).

Tectonically, the Yellow Sea basins formed due to both India-Eurasia and Pacific-Eurasia plate interactions, which led to repeated extension and rifting since the Late Mesozoic (Ren et al., 2002). Extension-driven regional subsidence formed marginal basins in the Yellow Sea (Watson et al., 1987). Since the Late Miocene, the Yellow Sea is thought to have undergone little to no tectonic subsidence, and, at the least, has not experienced uplift (Chough et al., 2000; Li et al., 2016). In the eastern Yellow Sea, the Korean Peninsula is characterized by rias and over 3000 islands along its western and southern coasts (Chough, 2013). The seafloor deepens progressively to the southeast along the NNW-SSE axis of the former Late Pleistocene lowstand shorelines (Fig. 1; Chough et al., 2000; 2004). Eustatic sea-level fluctuations during the Quaternary had a great effect on sedimentation in the Yellow Sea (Chough et al., 2000; Jin et al., 2002; Shinn et al., 2007; Yoo et al., 2016). Korean and Chinese onshore and offshore drill cores have revealed alternating terrestrial and shallow marine deposits formed during repeated Pleistocene transgressions and regressions (Li et al., 1991; Marsset et al., 1996; Jin et al., 2002; Chang et al., 2014; Li et al, 2016; S.H. Hong et al., 2019; H.H. Yoon et al., 2021). The present Yellow Sea formed during a large-scale Holocene transgression of the pre-Holocene terrestrial lowlands between Korea and China (Chough et al., 2000). Many vibracores and drill cores along the west coast of Korea sample those Holocene transgressive intertidal deposits unconformably overlying the pre-Holocene semi-consolidated, oxidized floodplain deposits, forming a retrograding, coarsening-upward succession (Y.A. Park et al. 1998; Y.H. Kim et al., 1999; Lim et al. 2004; K. Choi and Kim 2006; Chang et al., 2014; H.H. Yoon et al., 2021).

2.2 Overview of previous studies on the Korean Peninsula

We divided the east coast of the southern Korean Peninsula into two regions: the northern region extending from Gangneung through Uljin and to Yeongdeok (38° to 36.3°N) and the southern region extending from near Pohang to Ulju (36.3° to 35°N) (Fig. 2). Within the southern region, S.W. Kim (1973) was the first to publish ^{14}C ages from the marine terraces of Korea. He divided the marine terraces into 6 elevation groups ranging from 3 to 130 m above mean sea level (MSL) and suggested the highest two groups may have formed during a Pleistocene interglacial period. A separate study across much of the same region

by G.H. Oh (1977) divided the marine terraces into 3 elevation groups ranging from 10 to 80 m above MSL. When investigating
110 the same region, D.Y. Lee (1987) suggested that the marine terraces were divisible into 5 elevation groups ranging from 3 m
to 90 m above MSL. Based on their sedimentology and stratigraphy, D.Y. Lee (1987) suggested the highest, middle three, and
lowest groups of marine terraces formed during the Pliocene, Pleistocene, and Holocene, respectively.
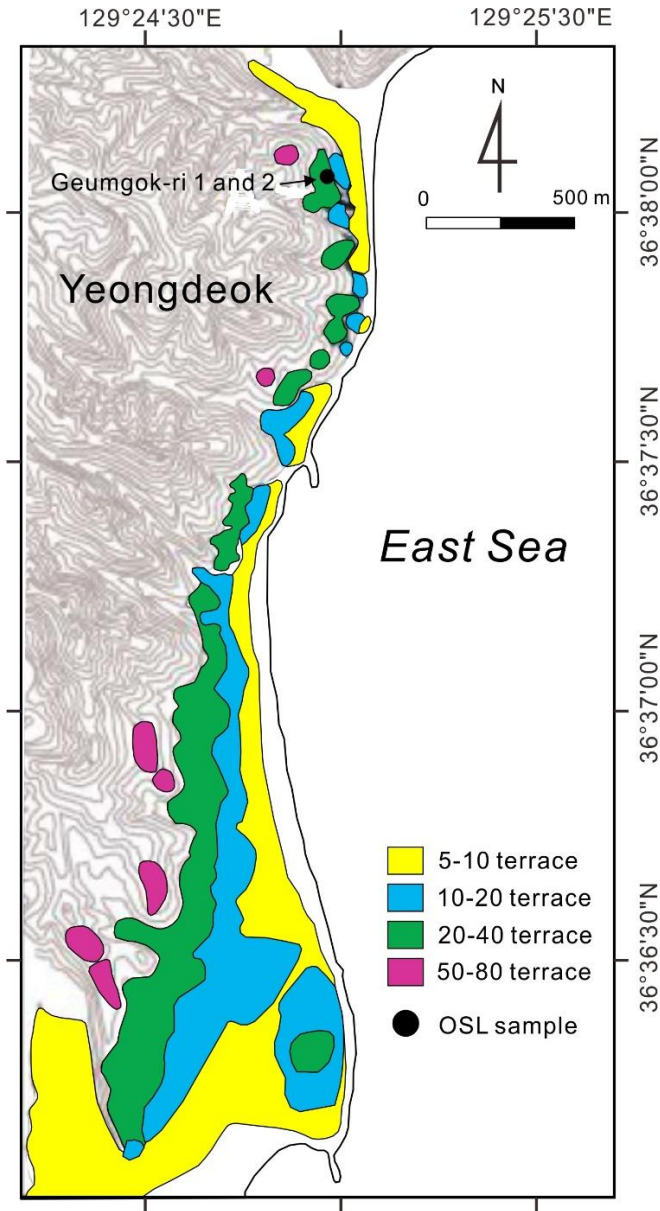
115 **Figure 3: Marine terraces at Subsite Geumgok-ri of the Yeongdeok area in the eastern Korean Peninsula (modified after S.C. Hong, 2014). The topographic contour interval is 10 meters. For location, see Fig. 2.**
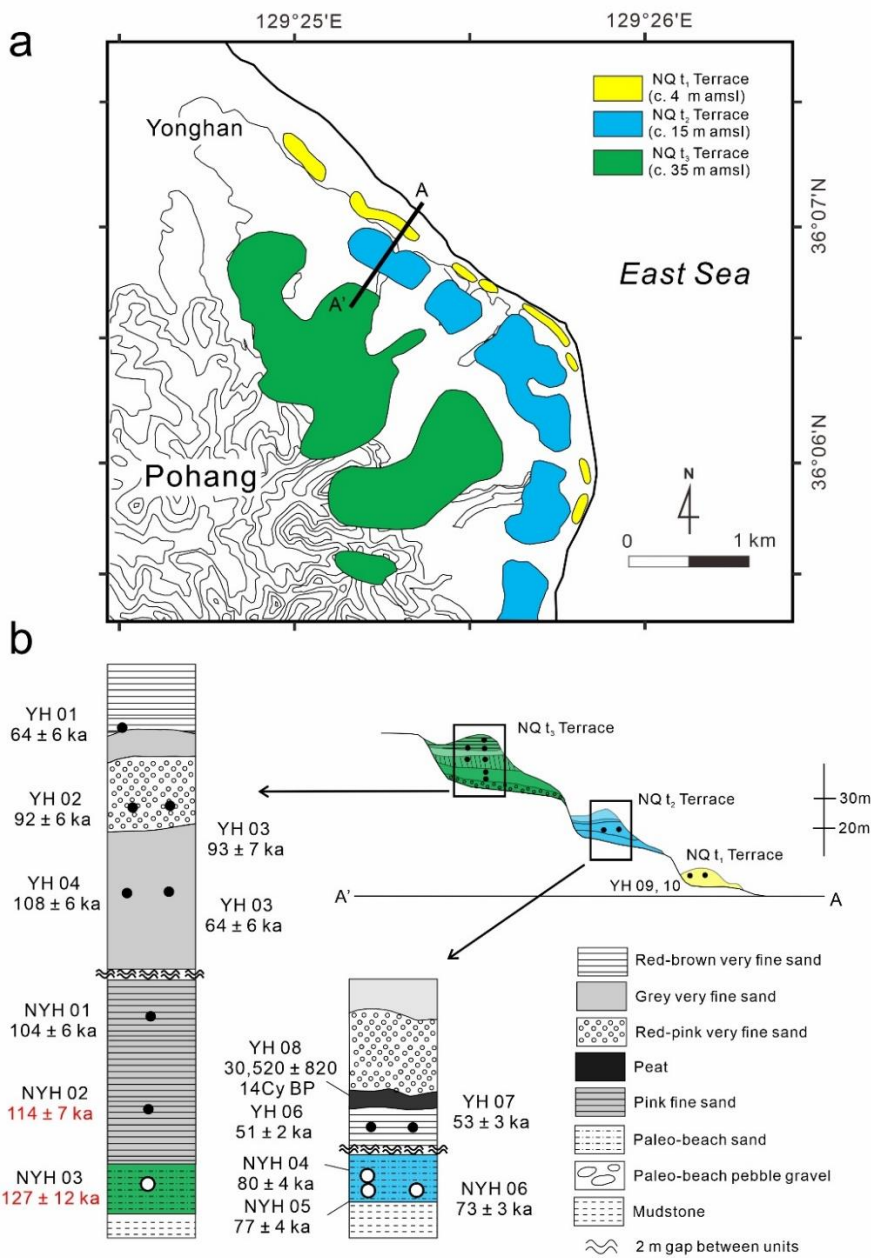
Figure 4: Marine terraces and columnar sections at Subsite Yonghan-2 of the Pohang area in the eastern Korean Peninsula (modified after J.H. Choi et al., 2009). (a) Plan view on the shoreline showing three ages of terraces. (b) Schematic cross-section and columnar sections of paleo-beach sediments overlain by aeolian sand on terraces. Open and closed circles indicate the location of OSL ages from paleo-beach and aeolian sand sediments, respectively. Two ages in red indicate LIG ages (WALIS LUM ID #449 and #450 in Table 3). Sites YH09 and YH10 in the NQt₁ terrace (yellow) were dated to 0.09±0.01 ka and 0.11±0.01 ka by OSL, respectively (J.H. Choi et al., 2009). The topographic contour interval is 10 meters. For location, see Fig. 2. amsl: above mean sea level
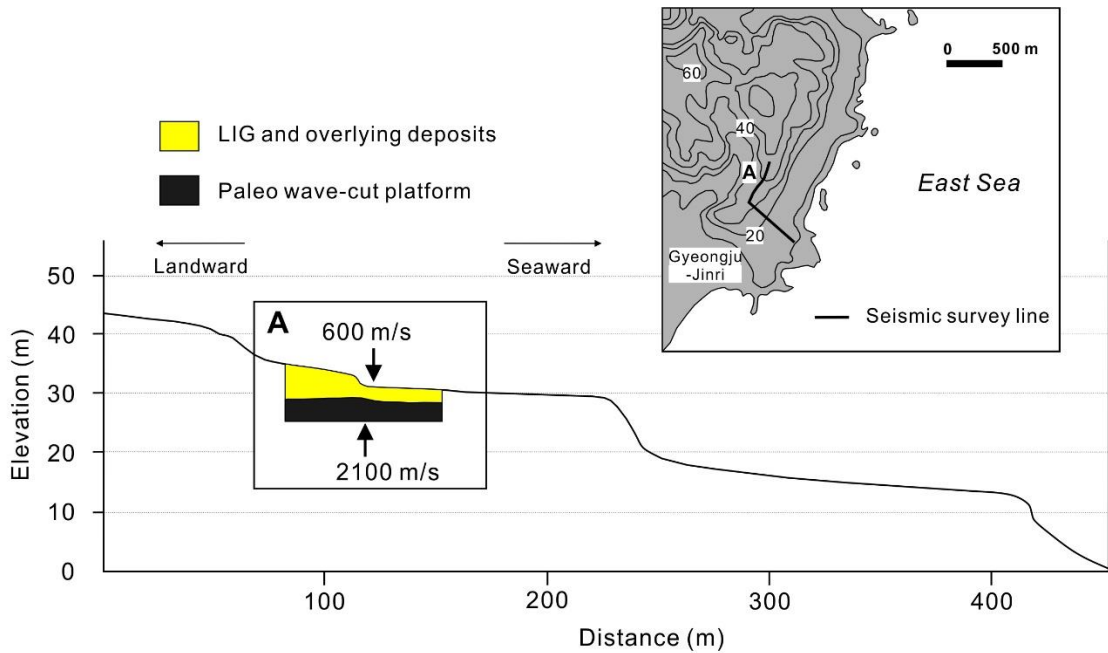
Figure 5: Seismic interpretation and calculated elevation of the buried LIG wave-cut platform at Subsite Jinri of the Gyeongju area, based on seismic velocities between the overlying deposits and a paleo wave-cut platform (modified after J.W. Kim et al., 2007a). The topographic contour interval is 10 meters. For location, see Fig. 2.

130
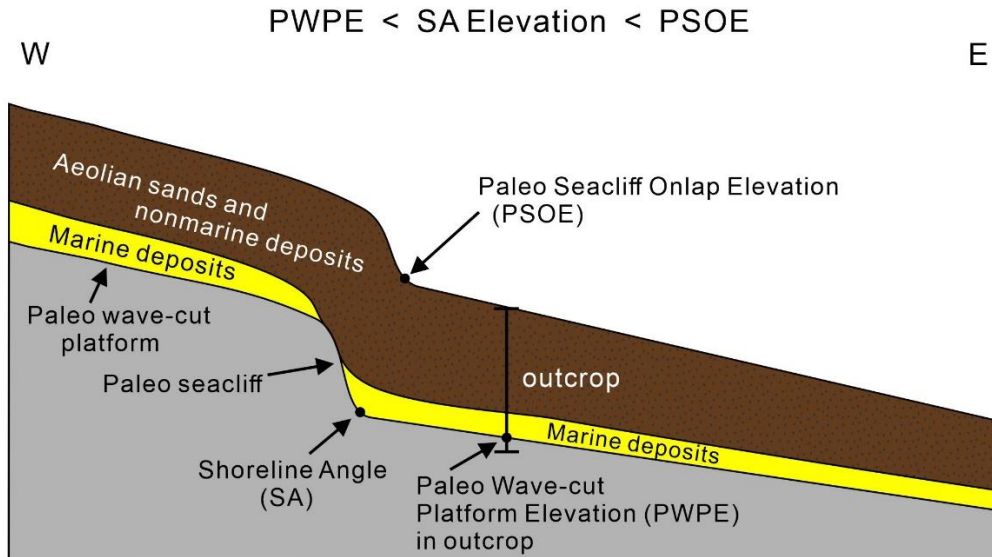
Figure 6: A schematic marine terrace commonly occurring along the eastern Korean Peninsula. Note that the shoreline angle (SA) elevation is between the paleo wave-cut platform elevation (PWPE) measured in outcrop and the paleo seacliff onlap elevation (PSOE) measured in surface topography.

135
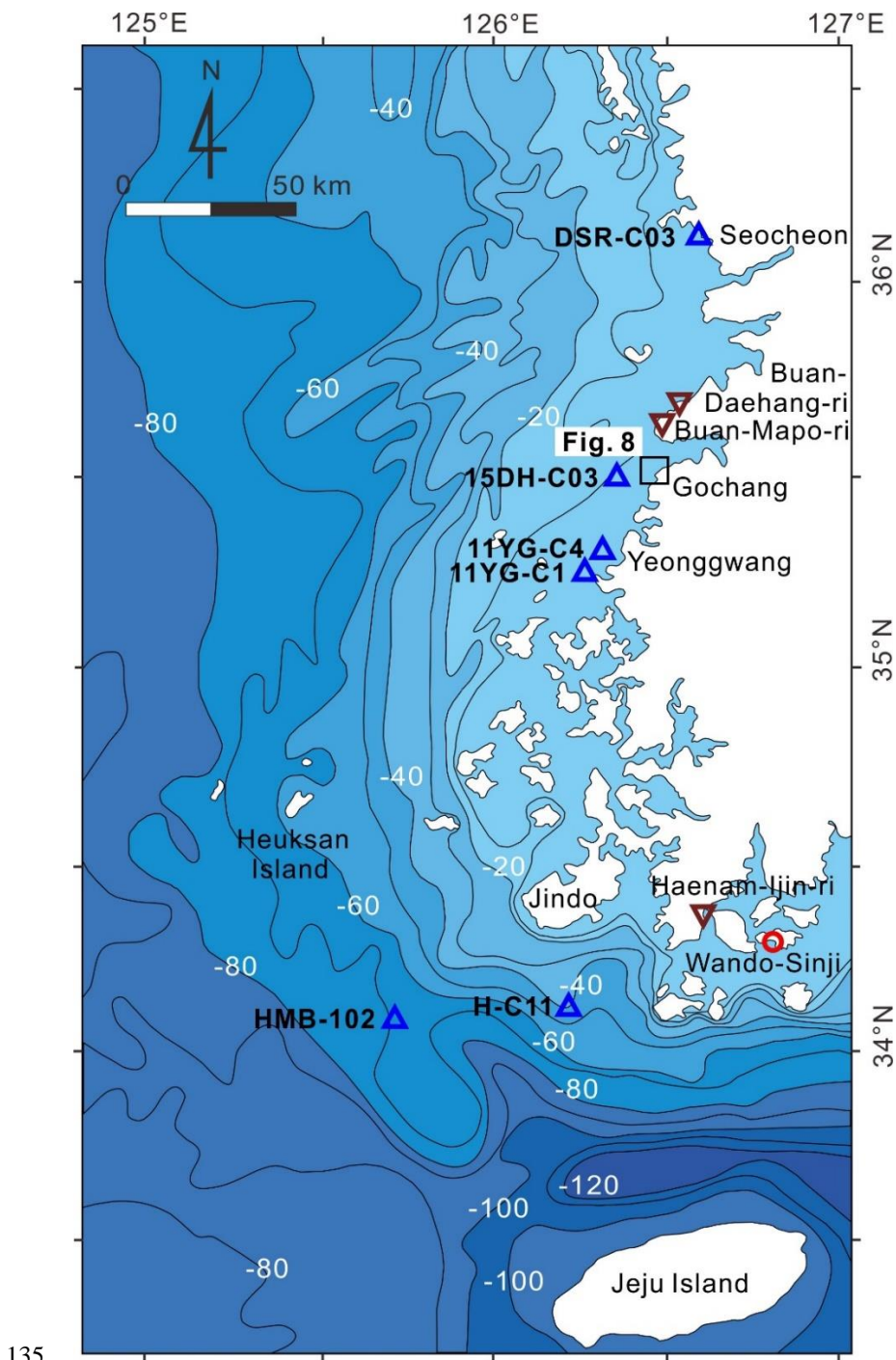
Figure 7: Location of nearshore drill cores and onshore sites in the western Korean Peninsula. A red circle represents the location of sea-level indicator while blue triangles and brown inverted triangles represent marine-limiting and terrestrial-limiting site locations, respectively. Age data can be found in Table 3. Bathymetric contour inveral is in meters.
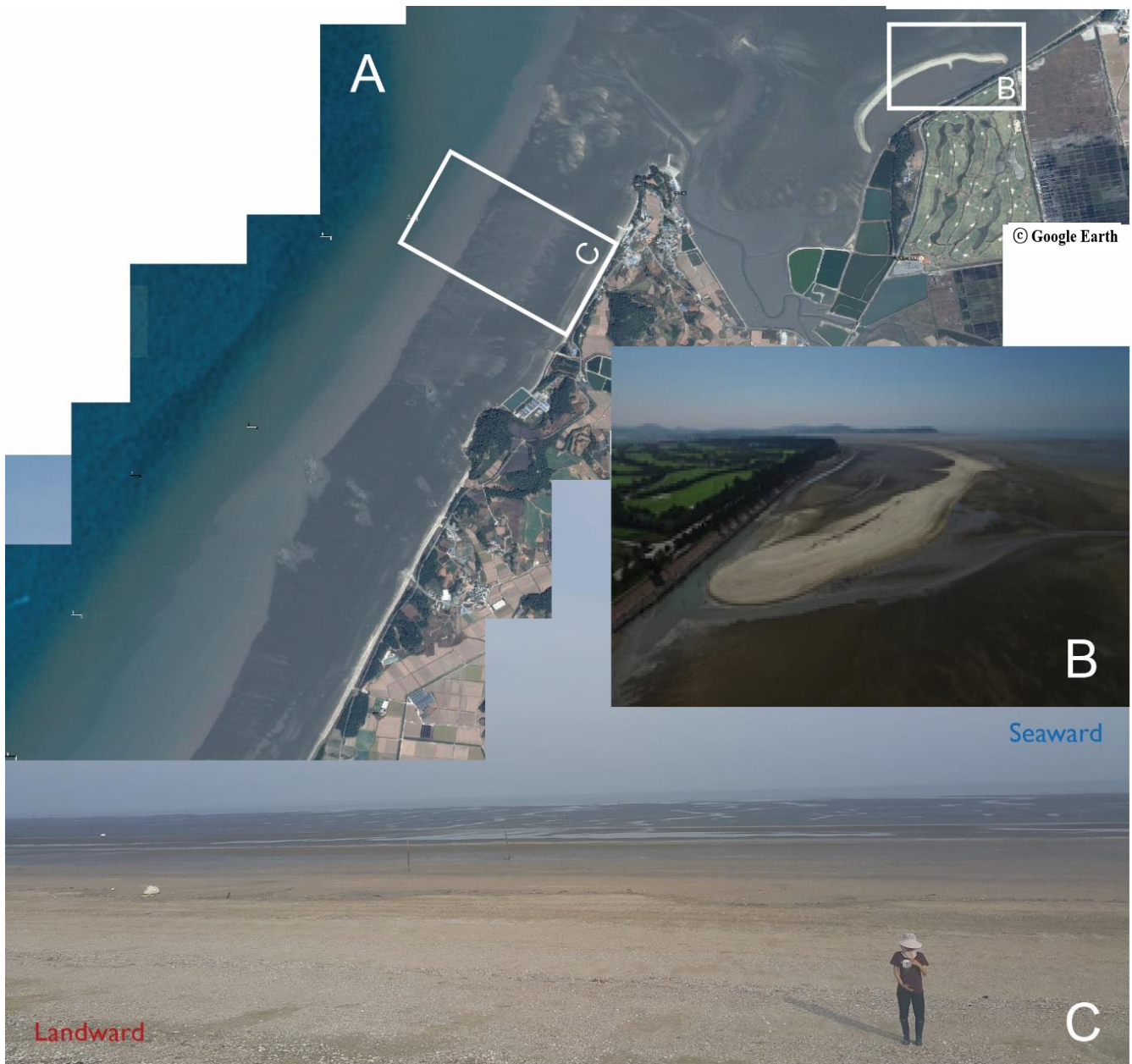
Figure 8: High-tide beaches, multiple swash bars, cheniers, and sandy tidal-flat deposits within the intertidal zone of the open coast along the western Korean coast (modified after Chun et al., 2018). (a) A satellite image with insets of landscape photographs in the Gochang area (from ©Google Earth), (b) A chenier on the tidal flat (Chun et al., 2018), (c) A high-tide beach of coarse sand and middle- to low-tide intertidal flats of muddy fine sand. The 2.0 ~ 3.0 ∅ sand predominantly fines seaward. For location, see Fig. 7.

145   In the northern region, the first LIG age (124 ka B.P.) was obtained from a fluvial terrace in the downstream part of the Seomseok river, located in Gangneung (Fig. 2), using amino acid racemization dating of peats (S.G. Choi, 1993). In the southern region, another LIG age (125 ka B.P.) was obtained from a separate fluvial terrace, located near the Pohang shoreline (Fig. 2), using the same method (S.G. Choi, 1996). However, due to inadequate descriptions of the sampled materials and age dating techniques within the original papers, the two ages were not included in our dataset shown in Table 3 or in the open-
150   access spreadsheet (Ryang and Simms, 2021). Since this initial work, most research has focused not on numerical dating, but documenting the elevations, sedimentary characteristics, and stratigraphy of deposits overlying the marine terraces along the eastern shorelines (e.g., S.G. Choi, 1995a, 1995b, 2016a, 2016b, 2018, 2019; S.G. Choi and Chang, 2019; Hwang and Yoon, 1996, 2020; Hwang et al., 2012; S.O. Yoon et al., 1999, 2003, 2014).

    In the 2000s, OSL dating started to be applied to the sandy deposits overlying the marine terraces of the eastern Korean
155   Peninsula. The first numerical age derived by OSL dating of paleo-beach sediments overlying a marine terrace was obtained near the Ulju shoreline within the southern region (dated to 112±7 ka) (J.H. Choi et al., 2003). Other studies soon added more OSL ages on the LIG marine terraces along the eastern shoreline of the Korean Peninsula (J.H. Choi, 2004; J.W. Kim et al., 2005a, 2007a, 2007b; S.J. Choi et al., 2008; S.C. Hong, 2014; S.Y. Lee et al., 2015; S.J. Choi, 2016; C.S. Park et al., 2017; G.Y. Lee and Park, 2019b).

160   Shim (2006) applied paleomagnetic analysis to outcrop sections of paleo-beach sand overlying a marine terrace along the Pohang shoreline within the southern region (Fig. 2), which was interpreted as MIS 5e deposits (114 to 120 ka). Tephrochronology and tephrostratigraphic correlation methods have also been used to suggest an MIS 5e age on deposits overlying a marine terrace at an elevation 15-20 m above MSL in the Gyeongju area of the southern region (Fig. 2; Inoue et al., 2002), but the age interpretation was quickly challenged because the dated deposits may have been reworked from
165   sediments of a higher terrace (S.J. Choi, 2003, 2009; S.J. Choi et al., 2008).

    Other efforts have been underway to identify LIG marine terraces or shoreline deposits along the southern and western shorelines of the Korean Peninsula (Lee G.Y. and Park, 2006; S.G. Choi, 2006; J.H. Yang, 2008, 2011; J.H. Yang et al., 2013; S.O. Yoon et al., 2015; W.J. Shin et al., 2016; J.S. Oh, 2018; Lee G.Y. and Park, 2018). However, most of these studies relied on elevation or stratigraphic correlation in the absence of numerical ages or analyzed the alluvial deposits overlying the
170   shoreline deposits. Recently, LIG shoreline deposits were discovered on the basis of OSL ages in the Sacheon, Wando, and Haenam areas (Figs. 2, 7; D.Y. Yang et al., 2016; J.Y. Shin, 2018; G.Y. Lee and Park, 2018, 2019a; W.J. Shin et al., 2019). Arguably the best sea-level constraints from these studies are those of W.J. Shin et al. (2019). W.J. Shin et al. (2019) identified paleo-intertidal/beach deposits composed of alternating gravel and sand beds with shell fragments along the southwest Korean shoreline near the Wando shoreline (Fig. 7). Their OSL ages were obtained from intertidal/beach deposits and dated to between
175   115.9 ± 9.7 and 127.5 ± 8.5 ka at an elevation of 3.5 to 2.8 m above MSL (W.J. Shin et al., 2019).

3 Methods

3.1 Elevation details

3.1.1 Datums

The Korean geodetic horizontal point is based on the World Geodetic Reference System (ITRF2000 & GRS80). This horizontal and vertical datum has been well managed for the national territory by the National Geographic Information Institute (2021). The Korean official vertical datum is based on mean sea level within Incheon Bay from 1913 to 1916 (Fig. 1). Using this datum, the institute installed a series of nationally unified control points and benchmarks across the entire Korean peninsula and territorial islands. All elevation data in this paper were measured using this national geodetic system.

3.1.2 Elevation measurements

All surveys include GPS or DGPS surveying methods. Most surveys also used an electro-optical distance measuring system (total station) to determine the elevation at specific points from a local benchmark of the Korean official vertical datum. Some locations were determined by comparing the GPS coordinates of the sampling point with a 1:5000 topographic map. Marine surveys used a virtual reference station linked to a GPS (VRS-GPS) or DGPS and a high-resolution echosounder aboard the drilling ship.

3.2 Coring

Cores were acquired using a hydraulic-powered drill on a barge or a vibrocorer deployed from a ship. Sediment sampling was performed using a standard thin-walled 55-mm diameter tube sampler. In the laboratory, cores were split lengthwise, described, photographed, and sampled. Core descriptions were based on sediment characteristics, including color, lithology, texture, grain size, and structure.

3.3 Dating techniques

3.3.1 Optically stimulated luminescence

Sixty-one of the 62 numerical ages in this dataset were acquired using OSL. Fifty-one OSL age measurements were conducted on coarse-grained sand or fine-grained silt quartz separates. Seven additional ages were obtained from K-feldspar minerals (IRSL, Infrared Stimulated Luminescence) isolated from coarse-grained sand and another 3 ages were obtained from K-feldspar minerals of gravel surfaces (rock surface OSL dating) (e.g., J.H. Choi et al., 2004; S.C. Hong et al., 2013; S.C. Hong, 2014, 2016). All OSL ages were conducted using the single-aliquot regenerative-dose (SAR) procedure (Murray and Wintle 2000) with error ranges listed as either ± 1σ SE or ± 2σ SE in accordance with the original studies.

3.3.2 Paleomagnetism

For the paleomagnetic study, sediment samples were collected almost continuously from an outcrop using non-magnetic 22 ×

205   22 × 22 mm^3 plastic cubes. The remanent magnetic moment of each sample was measured by a high-temperature superconducting magnetometer (F.I.T Messtechnik GmbH, HSM2) at Hanyang University (Shim, 2006). Alternating field demagnetization (Molspin Co.) and anhysteric/isothermal remanent magnetization experiments were performed to isolate the characteristic remanent magnetization of each sample (Shim, 2006). Magnetic susceptibility was measured by a susceptibility meter (Bartington Co., MS2F) for determining the types and amounts of ferrimagnetic minerals in the sediments.

210   3.3.3 Relative sea-level elevation assignments

3.3.3.1 Paleo sea level from marine terraces

The approach used to reconstruct paleo RSLs is in part dependent on the landform used (Tables 1, 2). The most commonly applied approach to reconstructing past RSLs from marine terraces is to use the elevation of the shoreline angle (SA in Fig. 6; "inner edge" of Bradley and Griggs, 1976 or junction between the marine platform and the paleo sea cliff of Muhs et al., 1990)

215   as a proxy for paleo sea levels. Unfortunately for most of the data collected to date across the marine terraces of the east coast of the Korean Peninsula, the shoreline angle (SA) elevation is unknown because the paleo-sea cliffs are covered by overlying deposits (Fig. 6). On the only 2 among the 13 subsites along the east coast (Fig. 2), the SA elevations of the marine terraces were measured in the original studies (Table 2; Fig. 5). In the case of an unknown shoreline angle elevation but where a paleo wave-cut platform elevation (PWPE) and a paleo seacliff onlap elevation (PSOE) were measured (Table 2; Fig. 6), we

220   expressed the estimated shoreline angle elevation (SA$_e$) as the mid-point elevation between the PWPE and the PSOE with an error range (δ_{SAe}) of ½ that elevation difference according to the following equations:

$$SA_e = \frac{(PSOE + PWPE)}{2} \tag{1}$$

$$\delta_{SAe} = \frac{(PSOE - PWPE)}{2} \tag{2}.$$

This approach allowed us to estimate RSLs from three additional subsites where the PWPE and the PSOE were measured in

225   the field (Table 2; Fig. 6).

RSL is calculated from all sea-level indicators using the following equations:

$$\text{Paleo RSL} = E - RWL \pm \frac{\delta_{RSL}}{2} \tag{3}$$

Where E represents the elevation of the sea-level indicator, RWL represents the reference water level, and δ_{RSL} accounts for the uncertainties in the paleo RSL (Rovere et al., 2016). Furthermore,

230    $$RWL = \frac{U_l + L_l}{2} = \frac{SWSH + d_b}{2} \tag{4}$$

where U$_l$ represents the upper limit of the modern analogue landform's elevation, L$_l$ represents the lower limit of the modern analogue landform's elevation, SWSH represents storm wave swash height, and d$_b$ represents the breaking depth. Each of these values was obtained from local sources (Table 1). Breaking depth was approximated using the following equation:

$$d_b = -\frac{H_s}{0.78} \tag{5}$$

where H_s represents an average significant wave height during one year with the constant 0.78 commonly used for wave breaking criteria on a smooth, flat slope (Table 1; U.S. Army Corps of Engineers, 1984; Rovere et al., 2016). The uncertainty in the paleo RSL (δ_{RSL}) was determined via:

$$\delta_{RSL} = \sqrt{E_e^2 + \left(\frac{IR}{2}\right)^2} = \sqrt{E_e^2 + \left(\frac{U_l - L_l}{2}\right)^2} = \sqrt{E_e^2 + \left(\frac{SWSH - d_b}{2}\right)^2} \tag{6}$$

where E_e and IR represent an error in the elevation measurement (standard deviation) and the indicative range, respectively (Rovere et al., 2016). For the case of marine terraces whose shoreline angle was measured or estimated, their RSL equivalent (Paleo SA RSL) would be:

$$\text{Paleo SA RSL} = \frac{PSOE + PWPE}{2} - RWL \pm \left(\frac{\delta_{RSL}}{2} + \frac{PSOE - PWPE}{2}\right) \tag{7}.$$

In cases along the east coast of the Korean Peninsula where both the elevation of the shoreline angle or paleo wave-cut platform are unknown, we base our estimates of RSL by treating the dated deposits overlying the marine terraces as beach sands using Eq. 8 such that

Paleo RSL at marine-terrace data points (Landform Type 1 in Table 1)

$$= E - RWL \pm \sqrt{E_e^2 + \left(\frac{SWSH - d_b}{2}\right)^2} \tag{8}.$$

Similar to the earlier estimates, we also used the local storm wave swash height (SWSH), average significant wave heights (H_s), and breaking depths (d_b) to calculate 30 paleo RSLs from the elevations of the beach sands overlying the marine terraces along the east coast (Table 3).

Table 1. Landforms used for calculating paleo relative sea level in this study.

Type	Landform	Upper limit	Lower limit	Definitions and Data
1	Beach sands overlying marine terraces ("marine terraces" of Rovere et al., 2016)	Storm Wave Swash Height (SWSH)	Breaking depth (d_b)	**MHHW**: mean higher high water, the average of the higher high water height of each tidal day (Pugh and Woodworth, 2014) **MLLW**: mean lower low water, the average of the lower low water height of each tidal day (Pugh and Woodworth, 2014)
2	Beach deposits (Rovere et al., 2016)	Ordinary berm (ob)	Breaking depth (d_b)	This study used the average heights of statistically estimated MHHW and MLLW of each tidal day observed during January, February, and March 2021 in the nearest station from the shoreline at each subsite (KHOA, 2021)
3	Beach rock (Rovere et al., 2016)	Spray zone (sz)	Breaking depth (d_b)	**SWSH**: storm wave swash height, the maximum elevation reached by extreme storms on the beach (Otvos, 2000)
4	Tidal-flat clastic deposits	Spray zone (sz)	Sum of mean lower low water and breaking depth (MLLW + d_b)	**H_s**: average significant wave height during one year (U.S. Army Corps of Engineers, 1984) This study used the maximum wave height for SWSH and average significant wave height for H_s observed during 2020 in the nearest station from the shoreline at each subsite (KHOA, 2021).

d_b: breaking depth, for a smooth, flat slope, $d_b = - H_s/0.78$ (U.S. Army Corps of Engineers, 1984)

ob: ordinary berm height, ob = 0.2 x H_s + MHHW (Mayer and Kriebel, 1994)

sz: spray zone height, sz = 2 x ob (Rovere et al., 2016)

255   **Table 2. Summary of shoreline angle elevations along the east coast of the Korean Peninsula.**

No.	Site	Subsite	Sample latitude (°)	Sample longitude (°)	Landform Type in Table 1	Shoreline angle elevation (m)	± Error ragne (m)	Measured elevation of paleo wave-cut platform (PWPE) (m)	Measured elevation of paleo seacliff onlap (PSOE) (m)	Topographic elevation range of paleo-shoreline deposits (m)	Reference
1	Gangneung	Anin	37.7401	128.9716	1	27.5	2.5	21.1	30	20~30	S.Y. Lee et al., 2015
2	Donghae	Eodal-dong	37.5657	129.1181	1	28.0	2.0	26.0	30	25~30	S.C. Hong, 2014
3	Pohang	Yongha n-2	36.1085	129.4230	1	35.0	-	34.4	?	?	J.H. Choi et al., 2009
4	Pohang	Masan-ri	36.0152	129.4826	1	23.5	1.5	22.0	25	10~25	J.W. Kim et al., 2005b
5	Gyeongju	Jinri	35.6827	129.4686	1	28.0	1.0	27~29	45	30~45	J.W. Kim et al., 2007a

Table 3. Summary of LIG relative sea levels and ages as data points in the Korean Peninsula. For references, refer to the text. SLI: sea level indicator; TL: terrestrial limiting record; ML: marine limiting record.

WALIS LUM ID	Site	Subsite	Sample latitude (°)	Sample longitude (°)	Indicator Type	Landform type in Table 1	Paleo RSL (m)	± Error of paleo RSL	Elevation above MSL (m)	Dating method	OSL mineral type	Age (ka)	± Age uncertainty (ka) and error range
432	Gang neung	Saemok ee	37.7402	128.9716	SLI	1	26.9	2.2	29.7	OSL	K-Feldspar	128.3	24.5 ± 1σ SE
433	Gang neung	Saemok ee	37.7402	128.9716	SLI	1	26.9	2.2	29.7	OSL	K-Feldspar	124.1	25.3 ± 1σ SE
434	Gang neung	Saemok ee surface age	37.7402	128.9716	SLI	1	25.9	2.2	28.7	OSL	K-Feldspar (gravel surface)	133.7	13.9 ± 1σ SE
435	Gang neung	Anin	37.7401	128.9716	SLI	1	20.3	2.2	23.08	OSL	Quartz	117.0	6.0 ± 1σ SE
436	Gang neung	Anin	37.7401	128.9716	SLI	1	20.3	2.2	23.09	OSL	Quartz	129.0	8.0 ± 1σ SE
492	Dong hae	Eodal-dong 1	37.5657	129.1181	SLI	1	27.4	2.2	30.2	OSL	Quartz	126.1	10.1 ± 1σ SE
437	Dong hae	Eodal-dong 1	37.5657	129.1181	SLI	1	27.4	2.2	30.2	OSL	K-Feldspar	127.5	24.6 ± 1σ SE
438	Dong hae	Eodal-dong 2	37.5657	129.1181	SLI	1	26.4	2.2	29.2	OSL	Quartz	128.0	14.0 ± 1σ SE
439	Dong hae	Eodal-dong 2	37.5657	129.1181	SLI	1	26.4	2.2	29.2	OSL	K-Feldspar	124.1	23.7 ± 1σ SE
440	Dong hae	Eodal-dong 3	37.5657	129.1181	SLI	1	25.4	2.2	28.2	OSL	Quartz	112.1	7.7 ± 1σ SE
441	Dong hae	Eodal-dong 3	37.5657	129.1181	SLI	1	25.4	2.2	28.2	OSL	K-Feldspar	125.3	24.0 ± 1σ SE
442	Uljin	Hujeong 1 (Gwang yoon Apt.)	37.0619	129.4153	SLI	1	28.2	1.7	30	OSL	Quartz	119.0	15.0 ± 1σ SE
443	Uljin	Hujeong 2 (Gwang yoon Apt.)	37.0619	129.4153	SLI	1	32.2	1.7	34	OSL	Quartz	111.0	9.0 ± 1σ SE
444	Yeon gdeok	Geumgo k-ri 1	36.6362	129.4150	SLI	1	19.4	1.7	21.2	OSL	K-Feldspar	124.5	25.3 ± 1σ SE
445	Yeon gdeok	Geumgo k-ri 2	36.6362	129.4150	SLI	1	22.1	1.7	23.9	OSL	K-Feldspar	122.1	24.9 ± 1σ SE

446	Pohang	Josa-ri	36.2194	129.3801	SLI	1	20.2	1.7	22	OSL	Quartz	116.0	8.0 ± 1σ SE
447	Pohang	Ohdo-ri	36.1586	129.3969	SLI	1	23.4	1.7	25.23	OSL	Quartz	137.0	9.0 ± 1σ SE
448	Pohang	Yonghan-1 (silica mine)	36.1093	129.4161	SLI	1	30.2	1.7	32	OSL	Quartz	123.0	9.0 ± 1σ SE
449	Pohang	Yonghan-2a	36.1085	129.4230	TL	1	33.7	1.7	35.5	OSL	Quartz	114.0	7.0 ± 1σ SE
450	Pohang	Yonghan-2b	36.1085	129.4230	SLI	1	33.2	1.7	35	OSL	Quartz	127.0	12.0 ± 1σ SE
451	Pohang	Masan-ri	36.0152	129.4826	SLI	1	21.2	1.7	23	OSL	Quartz	119.0	8.0 ± 1σ SE
452	Pohang	Masan-ri	36.0152	129.4826	SLI	1	21.7	1.7	23.5	OSL	Quartz	111.0	5.0 ± 1σ SE
453	Pohang	Masan-ri	36.0152	129.4826	SLI	1	22.2	1.7	24	OSL	Quartz	116.0	7.0 ± 1σ SE
454	Pohang	Masan-ri	36.0152	129.4826	SLI	1	22.7	1.7	24.5	OSL	Quartz	107.0	8.0 ± 1σ SE
–	Pohang	Masan-ri	36.0152	129.4826	SLI	1	21.2	1.7	23	Paleomagnetism	–	117.6	2.7 ± 1σ SE
455	Pohang	Hajeong-ri	35.9716	129.5493	TL	1	33.2	1.7	35	OSL	Quartz	128.0	12.0 ± 2σ SE
456	Gyeongju	Jinri	35.6827	129.4686	SLI	1	32.3	2.6	36	OSL	Quartz	116.0	6.0 ± 1σ SE
457	Gyeongju	Jinri	35.6827	129.4686	SLI	1	32.3	2.6	36	OSL	Quartz	126.0	10.0 ± 1σ SE
459	Ulsan	Jeongja-ri	35.6311	129.4331	SLI	1	18.8	2.6	22.5	OSL	Quartz	113.0	39.0 ± 1σ or 2 σ SE
458	Ulju	Weseong	35.3821	129.3414	SLI	1	10.3	2.6	14	OSL	Quartz	112.0	7.0 ± 1σ SE
460	Sacheon	Daepo-dong	34.9900	128.0427	SLI	2	6.0	0.8	6	OSL	K-Feldspar (cobble surface)	111.2	16.0 ± 1σ SE
461	Sacheon	Daepo-dong	34.9900	128.0427	SLI	2	6.0	0.8	6	OSL	K-Feldspar (cobble surface)	102.5	14.7 ± 1σ SE
462	Wando	Sinji 1	34.3258	126.8286	SLI	2	2.5	0.9	2.8	OSL	Quartz	127.5	8.5 ± 1σ SE

463	Wando	Sinji 1	34.3258	126.8286	SLI	2	3.2	0.9	3.5	OSL	Quartz	115.9	9.7 ± 1σ SE
464	Wando	Sinji 3	34.3280	126.8258	SLI	2	5.8	0.9	6.1	OSL	Quartz	108.0	18.0 ± 1σ SE
465	Haenam	Ijin-ri 1	34.3962	126.6175	TL	3	6.4	1.3	7.51	OSL	Quartz	121.0	10.0 ± 2σ SE
466	Haenam	Ijin-ri 2	34.3962	126.6175	TL	3	5.3	1.3	6.49	OSL	Quartz	128.0	10.0 ± 2σ SE
467	Haenam	Ijin-ri 3	34.3962	126.6175	TL	3	4.3	1.3	5.41	OSL	Quartz	128.0	9.0 ± 2σ SE
468	Buan	Daehang-ri	35.6790	126.5312	TL	3	8.2	2.0	10.78	OSL	Quartz	112.0	24.0 ± 1σ SE
469	Buan	Mapo-ri	35.6523	126.5073	TL	3	6.2	2.0	8.8	OSL	Quartz	130.0	20.0 ± 1σ SE
470	Seocheon	Dasa-ri 1	36.1043	126.6078	ML	4	-3.8	2.5	-1.88	OSL	Quartz	116.0	10.0 ± 1σ SE
471	Seocheon	Dasa-ri 2	36.1043	126.6078	ML	4	-5.7	2.5	-3.82	OSL	Quartz	108.0	8.0 ± 1σ SE
472	Yeonggwang	Baeksu 1	35.3032	126.3212	ML	4	-22.8	2.5	-20.8	OSL	Quartz	110.0	6.6 ± 2σ SE
473	Yeonggwang	Baeksu 2	35.3032	126.3212	ML	4	-24.1	2.5	-22.1	OSL	Quartz	133.9	7.6 ± 2σ SE
474	Yeonggwang	Baeksu 3	35.3032	126.3212	ML	4	-25.9	2.5	-23.9	OSL	Quartz	124.0	7.8 ± 2σ SE
475	Yeonggwang	Baeksu 4	35.3032	126.3212	ML	4	-27.2	2.5	-25.2	OSL	Quartz	138.8	7.8 ± 2σ SE
476	Yeonggwang	Baeksu 5	35.3032	126.3212	ML	4	-28.8	2.5	-26.8	OSL	Quartz	128.7	7.9 ± 2σ SE
477	Yeonggwang	Baeksu 6	35.3032	126.3212	ML	4	-30.3	2.5	-28.3	OSL	Quartz	124.7	7.6 ± 2σ SE
478	Yeonggwang	Baeksu 7	35.3032	126.3212	ML	4	-31.8	2.5	-29.8	OSL	Quartz	118.8	7.0 ± 2σ SE
479	Yeonggwang	Baeksu 8	35.3032	126.3212	ML	4	-33.3	2.5	-31.3	OSL	Quartz	112.2	6.8 ± 2σ SE

480	Yeon ggwa ng	Baeksu 9	35.3032	126.3212	ML	4	-34.8	2.5	-32.8	OSL	Quartz	113.4	7.1 ± 2σ SE
481	Yeon ggwa ng	Baeksu 10	35.3032	126.3212	ML	4	-36.3	2.5	-34.3	OSL	Quartz	118.2	7.4 ± 2σ SE
482	Yeon ggwa ng	Baeksu 11	35.3032	126.3212	ML	4	-37.8	2.5	-35.8	OSL	Quartz	112.6	6.9 ± 2σ SE
483	Yeon ggwa ng	Baeksu 12	35.3032	126.3212	ML	4	-39.3	2.5	-37.3	OSL	Quartz	113.1	7.3 ± 2σ SE
484	Yeon ggwa ng	Baeksu-Duuri 1	35.2723	126.2845	ML	4	-17.4	2.5	-15.48	OSL	Quartz	107.7	6.7 ± 2σ SE
485	Yeon ggwa ng	Baeksu-Duuri 2	35.2723	126.2845	ML	4	-27.9	2.5	-25.98	OSL	Quartz	122.1	7.2 ± 2σ SE
486	Yeon ggwa ng	Baeksu-Duuri 3	35.2723	126.2845	ML	4	-29.2	2.5	-27.28	OSL	Quartz	126.2	8.1 ± 2σ SE
487	Gocha ng	Dongho 1	35.4911	126.3678	ML	4	-37.2	2.5	-35.2	OSL	Quartz	107.5	7.6 ± 2σ SE
488	Gocha ng	Dongho 2	35.4911	126.3678	ML	4	-39.4	2.5	-37.4	OSL	Quartz	107.6	7.3 ± 2σ SE
489	Gocha ng	Dongho 3	35.4911	126.3678	ML	4	-40.2	2.5	-38.2	OSL	Quartz	113.3	7.2 ± 2σ SE
490	Jindo	Jindo shelf	34.1205	126.2188	ML	4	-49.0	1.5	-48.5	OSL	Quartz	124.4	10.0 ± 2σ SE
491	Heuks an Island	Heuksan Mud Belt	34.1326	125.6823	ML	4	-84.7	1.6	-84	OSL	Quartz	125.1	9.9 ± 2σ SE

260

3.3.3.2 Paleo sea level calculated from beach and tidal deposits

Beach deposits and beach rock are also a reliable RSL marker because the formative zone is in close proximity to sea levels (Mauz et al., 2015). Five paleo RSLs of beach deposits (Landform Type 2 in Table 1) and an additional five paleo RSLs of beach rock (Landform Type 3 in Table 1) were used to determine paleo RSLs from LIG-aged deposits along the western and

265   southern Korean coast. RSLs from beach rock were calculated using the following equations:

Paleo RSL at beach-deposit data points (Landform Type 2 in Table 1)

$$= E - RWL \pm \sqrt{E_e^2 + \left(\frac{ob - d_b}{2}\right)^2} = \sqrt{E_e^2 + \left(\frac{(0.2 * H_s + MHHW) - d_b}{2}\right)^2} \qquad (9)$$

where (ob) represents the ordinary berm height, which was estimated using the average significant wave height over one year (H_s) and MHHW represents the mean higher high water heights (Table 1; Mayer and Kriebel, 1994; Rovere et al., 2016). For

270 beach rocks, we used a similar expression:

Paleo RSL at beach-rock data points (Landform Type 3 in Table 1)

$$= \mathrm{E} - \mathrm{RWL} \pm \sqrt{E_e^2 + \left(\frac{sz - d_b}{2}\right)^2} = \sqrt{E_e^2 + \left(\frac{2 * (0.2 * H_s + MHHW) - d_b}{2}\right)^2} \qquad (10)$$

where (sz) represents the elevation of the top of the spray zone, which was calculated using the average significant wave height over one year (H_s) (Table 1; Rovere et al., 2016).

275   Twenty-two OSL-dated clastic tidal-flat deposits from nearshore cores were also used to estimate paleo RSLs based on Eq. (11).

Paleo RSL at tidal-flat clastic data points (Landform Type 4 in Table 1)

$$= \mathrm{E} - \mathrm{RWL} \pm \sqrt{E_e^2 + \left(\frac{sz - (MLLW + d_b)}{2}\right)^2} = \sqrt{E_e^2 + \left(\frac{2 * (0.2 * H_s + MHHW) - (MLLW + d_b)}{2}\right)^2} \qquad (11)$$

where MLLW represents mean lower low water heights (Table 1).

280   4   Relative Sea-level Indicators

In the following sections, we discuss each characteristic of the RSL indicators from the Korean Peninsula, identified by their 'WALIS RSL ID' in the text, which have been entered into the WALIS database. The ID number corresponds with the WALIS database identification numbers. Similarly, we use 'WALIS LUM ID' followed by a number to reference an optically stimulated luminescence (LUM) age within the database.

285   The east coast of the southern Korean Peninsula was divided into two regions, a northern and a southern region, based on latitude. The northern region encompasses the area from Gangneung through Uljin and the Yeongdeok area (38°N to 36.3°N) while the southern region encompasses the region between Pohang and Ulju (36.3°N to 35°N) (Fig. 2). Along the west and southwest coast of the southern Korean Peninsula, the sea-level data and indicators were divided into two groups, those found onshore and those found within the nearshore.

290   4.1 Marine terraces along the northern east coast

4.1.1 Gangneung area

Two areas have been studied within the Gangneung area: Gangneung-Saemokee and Gangneung-Anin (Fig. 2). The marine deposits overlying the paleo wave-cut platform of the marine terrace at Gangneung-Saemokee are found 27~31 m above MSL and contain rounded cobbles and some sand deposits of paleo beach origin (S.C. Hong, 2014). At Subsite Gangneung-

295 Saemokee, two quartz OSL ages were interpreted as minimum ages of >85 ka and >92 ka. These deposits appear to exceed

the upper age limit of the methodology because the signal is saturated (e.g., Rhodes, 2011). Fortunately, two IRSL ages of 128.3±24.5 ka (WALIS LUM ID #432) and 124.1±25.3 ka (WALIS LUM ID #433) and one cobble surface OSL age of 133.7±13.9 ka (WALIS LUM ID #434) were obtained from these terrace deposits (Table 3; S.C. Hong, 2014). Using Eq. (8), the paleo RSLs of these samples without a PWPE yielded 26.9±2.2 m, 26.9±2.2 m, and 25.9±2.2 m above MSL, respectively (Table 3; WALIS RSL ID #4009, 4010).

Gangneung-Anin is located 23 m above MSL and consists of beach sand and gravel deposits overlying a paleo wave-cut platform. The two ages from the beach sand were 117±6 ka (WALIS LUM ID #435) and 129±8 ka (WALIS LUM ID #436) (Table 3; S.Y. Lee et al., 2015). At this site, although the paleo shoreline angle elevation is unknown, we estimated the SA elevation to be approximately 27.5±2.5 m above MSL using a value of 25 m for PWPE and 30 m for PSOE in Eqs. (1) and (2) (Table 2; Fig. 6).

4.1.2 Donghae area

Donghae-Eodal-dong is located 26 m above MSL (Fig. 2) and consists of beach sand and pebble deposits overlying a paleo wave-cut platform. The three samples from the beach sand were analyzed using paired OSL and IRSL methods. The three OSL/IRSL age sets from the beach sand were 126.1±10.1 ka (OSL, WALIS LUM ID #492) and 127.5±24.6 ka (IRSL, WALIS LUM ID #437), 128±14 ka (OSL, WALIS LUM ID #438) and 124.1±23.7 ka (IRSL, WALIS LUM ID #439), and 112.1±7.7 ka (OSL, WALIS LUM ID #440) and 125.3±24 ka (IRSL, WALIS LUM ID #441) (Table 3; S.C. Hong, 2014). Using Eq. (8), the paleo RSLs of these samples without a PWPE yielded 27.4±2.2 m, 26.4±2.2 m, and 25.4±2.2 m above MSL, respectively (Table 3; WALIS RSL ID #4012, 4014, 4015). At this site, the paleo shoreline angle elevation is estimated to be 28±2 m above MSL using 26 m for PWPE and 30 m for PSOE (Table 2; Fig. 6).

4.1.3 Uljin area

Subsite Uljin-Hujeong is located 30~34 m above MSL (Fig. 2) and is comprised of moderately well-sorted sand (>5 m thick) with a mean grain size of ~ 1.3 φ overlying a paleo wave-cut platform (J.W. Kim et al., 2007b). The two OSL ages from the sand deposits were 119±15 ka (WALIS LUM ID #442) and 111±9 ka (WALIS LUM ID #443) (Table 3; J.W. Kim et al., 2007b). Without a PWPE we estimated RSL using Eq. (8) based on its use as a beach RSL indicator (Landform Type 1 in Table 1). For that calculation, we arrive at RSL estimates of 28.2±1.7 m and 32.2±1.7 m, respectively (Table 3; WALIS RSL ID #4016, 4017).

4.1.4 Youngduk area

Subsite Youngdeok-Geumgok-ri is located 20-25 m above MSL and contains rounded cobbles, pebbles, and sand deposits overlying a paleo wave-cut platform (Figs. 2, 3; S.C. Hong, 2014). Two OSL ages from quartz sand in the overlying marine deposits were interpreted as minimum ages of >44 ka and >41 ka. They appear to exceed the upper age limit of the methodology in these sediments as the traps are saturated (e.g., Rhodes, 2011). Two additional IRSL ages of 124.5±25.3 ka

(WALIS LUM ID #444) and 122.1±24.9 ka (WALIS LUM ID #445) were obtained from the sand deposits (Table 3; S.C. Hong, 2014). Without a PWPE we estimated RSL using Eq. (8) based on its use as a beach RSL indicator (Landform Type 1 in Table 1). For that calculation, we arrives at RSL estimates of 19.4±1.7 m and 22.1±1.7 m, respectively (Table 3; WALIS RSL ID #4018, 4019).

4.2 Marine terraces along the southern east coast

4.2.1 Pohang area

This area comprises six subsites at Pohang-Josa-ri, Pohang-Ohdo-ri, Pohang-Yonghan-1 (silica mine), Pohang-Yonghan-2, Pohang-Masan-ri, and Pohang-Hajeong-ri (Fig. 2). Subsite Pohang-Josa-ri is located 22 m above MSL and contains alternating beds (~1.5 m thick) of sand and silt overlying a paleo wave-cut platform (G.Y. Lee and Park, 2019b). The single OSL age from the sand deposits was 116±8 ka (WALIS LUM ID #446) (G.Y. Lee and Park, 2019b, 2020). Subsite Pohang-Ohdo-ri is located on a marine terrace 25.2 m above MSL and consists of well-rounded cobbles, pebbles, and sand (>3 m thick) (G.Y. Lee and Park, 2019b). The single OSL age from the sand deposits was 137±9 ka (WALIS LUM ID #447) (Table 3; G.Y. Lee and Park, 2019b, 2020). Treating the deposits as beach sands overlying marine terraces without a PWPE and using Eq. (8) we arrived at RSL estimates of 20.2±1.7 m and 23.4±1.7 m for subsites Pohang-Josa-ri and Pohang-Ohdo-ri, respectively (Table 3; WALIS RSL ID #4020, 4021).

Subsite Pohang-Yonghan-1 (silica mine) is located on a marine terrace 32 m above MSL and contains alternating well-rounded pebble and sand beds (~1.2 m thick) (J.W. Kim et al., 2005a). A single OSL age of 123±9 ka (WALIS LUM ID #448) was obtained from the sand deposits (J.W. Kim et al., 2005a). The paleo RSLs of this sample yielded 30.2±1.7 m above MSL using Eq. (8) (Table 3; WALIS RSL ID #4022).

Subsite Pohang-Yonghan-2 is located on top of a marine terrace 35 m above MSL and contains alternating paleo-beach beds (~0.5 m thick) of well-rounded pebble and sand overlain by aeolian sand beds (~8 m thick) (Fig. 4; J.H. Choi et al., 2009). The two ages from the paleo-beach sand sediments were 114±7 ka (WALIS LUM ID #449) and 127±12 ka (WALIS LUM ID #450) (Table 3; J.H. Choi et al., 2009). Using Eq. (8), the paleo RSLs of these samples without a PWPE yielded 33.2±1.7 m above MSL (Table 3; WALIS RSL ID #4024). The overlying aeolian sand beds returned younger OSL ages of 104±6 ka, 108±6 ka, 92±6 ka, and 64±6 ka (not included in WALIS) in ascending stratigraphic order (Fig. 4; J.H. Choi et al., 2009). The elevation of the LIG shoreline angle is 35 m above MSL (Table 2; Fig. 4; J.H. Choi et al., 2009).

Subsite Pohang-Masan-ri is located 23 m above MSL and contains paleo-beach sand beds (~0.24 m thick) and overlying aeolian sand beds (~5 m thick) above a paleo wave-cut platform (J.W. Kim et al., 2005b). The significance of the terraces in this region is also discussed by Thompson and Creveling (2021) who focus more on the MIS 5c and MIS 5a ages from this site and adjacent areas. The four OSL ages from the paleo-beach sand sediments were 119±8 ka (WALIS LUM ID #451), 111±5 ka (WALIS LUM ID #452), 116±7 ka (WALIS LUM ID #453), and 107±8 ka (WALIS LUM ID #454) (Table 3; J.W. Kim et al., 2005b). Using Eq. (8), the paleo RSLs of these samples without a PWPE yielded 21.2±1.7 m above MSL (Table 3;

WALIS RSL ID #4025). A total of 158 sediment samples were also collected almost continuously from approximately 3.8 m

of the Masanri (MS) outcrop section for a paleomagnetic study (Shim, 2006). Remanent magnetic moment, alternating field demagnetization, anhysteric/isothermal remanent magnetization, and magnetic susceptibility of each sample were measured to isolate characteristic remanent magnetization (Shim, 2006). The global Blake Excursion Event was discovered in the MS section on the Masan-ri marine terrace in the northern Pohang area (Fig. 2). The elevation of this outcrop section is 22 m above MSL. Considering the Blake Event (111.8 to 117.1 ka), the paleomagnetic age of the paleo-beach sediments overlying the marine terrace suggests a numerical age of 117.6±2.7 ka with an error range of between 114.9 and 120.2 ka (Table 3; Shim, 2006). At this site, the shoreline angle elevation is estimated to be 23.5±1.5 m above MSL using 22 m for PWPE and 25 m for PSOE (Table 2; Fig. 6).

Subsite Pohang-Hajeong-ri is located 35 m above MSL, and the section crops out in the footwall of the Hajeong fault. The section contains a wedge-shaped mix (98 to 20 cm thick) of rounded pebbles, sand, and angular alluvial pebbles overlying a marine terrace (S.J. Choi, 2016). The single OSL age from the sand was 128±12 ka (WALIS LUM ID #455) (Table 3; S.J. Choi, 2016), which is interpreted as a terrestrial limiting data point.

4.2.2 Gyeongju area

Subsite Gyeongju-Jinri is located on a marine terrace 36 m above MSL (Fig. 2) and contains thin (~ 15 cm thick) paleo-beach gravels underlying fine-grained sand beds (~0.5 m thick) (J.W. Kim et al., 2007a). The two OSL ages from the sand deposits were 116±6 ka (WALIS LUM ID #456) and 126±10 ka (WALIS LUM ID #457) (Table 3; J.W. Kim et al., 2007a). Using Eq. (8), the paleo RSLs of these samples without a PWPE yielded 32.3±2.6 m above MSL (Table 3; WALIS RSL ID #4027). In this area, a land seismic survey was conducted to identify the elevation of the buried paleo wave-cut platform and shoreline angle. Based on seismic velocities of 600 m/s for the overlying deposits and 2100 m/s for the wave-cut platform, the elevation of the paleo wave-cut platform ranges from 27 to 29 m above MSL with a slope of 1.5° (Fig. 5; J.W. Kim et al., 2007a). The shoreline angle elevation is estimated to be 28±1 m above MSL (Table 2).

4.2.3 Ulsan area

Subsite Ulsan-Jeongja-ri is located 19~28 m above MSL and contains a lower unit of fluvial beds (~2 m thick), a middle unit of fluvial/beach transitional beds (<1 m thick), and an upper unit of paleo-beach beds (~1 m thick) containing pebbles and sand overlying a paleo wave-cut platform (S.J. Choi et al., 2008). These terrace deposits are overlain by alternating alluvial beds (>2 m thick) of gravel, sand, and mud (S.J. Choi et al., 2008). The single OSL age from the sand deposits was 113±39 ka (WALIS LUM ID #459) (Table 3; S.J. Choi et al., 2008). Treating the sands as a beach deposit using Eq. (8) gives an RSL estimate of 18.8±2.6 m (Table 3; WALIS RSL ID #4028).

4.2.4 Ulju area

Subsite Ulju-Weseong contains well-sorted beach sand on a marine terrace at an elevation of 14 m above MSL (Fig. 2; J.H. Choi, 2004). The sand deposit was dated to 112±7 ka (WALIS LUM ID #458) (Table 3; J.H. Choi et al., 2003; J.H. Choi, 2004). Using Eq. (8), the paleo RSLs of these samples without a PWPE yielded 10.3±2.6 m above MSL (Table 3; WALIS RSL ID #4029). Thompson and Creveling (2021) discuss the sea-level significance of this site and adjacent areas in their summary of MIS5c and MIS5a sea levels.

4.3 Paleo-shoreline deposits between the east and west coasts

4.3.1 Sacheon area

The Sacheon area is located in the south-facing Korean Peninsula straddling the eastern and western coasts (Fig. 2). Subsite Sacheon-Daepo-dong lies at ~6 m above MSL and unlike the LIG shorelines of the eastern Korean Peninsula is not marked by a distinctive marine terrace geomorphology (J.Y. Shin and Hong, 2018). The paleo-shoreline deposits (2-3.5 m thick) are characterized by clast-supported well-rounded cobble and pebble deposits with little to no matrix. Their sedimentary characteristics are similar to the sandy gravel bars of the modern upper tidal flats in the region (J.Y. Shin and Hong, 2018). Two OSL rock-surface ages obtained from cobbles were 111.2±16.0 ka (WALIS LUM ID #460) and 102.5±14.7 ka (WALIS LUM ID #461) (Table 3; J.Y. Shin and Hong, 2018). Based on Eq. (9), we arrive at a RSL estimate of 6.0±0.8 m (Table 3; WALIS RSL ID #4030).

4.4 Onshore paleo-beach and terrestrial deposits of the west coast

4.4.1 Wando area

Subsite Wando-Sinji has two localities at approximately 3 m and 6 m above MSL (G.R. Lee and Park, 2018; W.J. Shin et al., 2019). At the 3 m site, a 0.3 to 1 m thick shell-bearing sand with well-rounded pebbles and cobbles is interpreted to represent a paleo-beach deposit. Its sedimentary facies is similar to the modern sandy gravel tidal-beach or intertidal deposits of the modern upper tidal flats of the region (W.J. Shin et al., 2019). The five OSL ages acquired from the deposits at 2.55, 2.80, 3.50, 4.25, and 4.50 m above MSL were 157.4±18.9, 127.5±8.5, 115.9±9.7, 23.2±1.2, and 6.2±0.4 ka, respectively (W.J. Shin et al., 2019). Only the two MIS 5e ages of 127.5±8.5 ka (WALIS LUM ID #462) and 115.9±9.7 ka (WALIS LUM ID #463) were included in the WALIS database (Table 3; W.J. Shin et al., 2019). Based on Eq. (9), we arrive at a RSL estimate of 2.5±0.9 m and 3.2±0.9 m (Table 3; WALIS RSL ID #4031).

At the 6 m locality, 4 m of sand and well-rounded cobbles and boulders are thought to represent a paleo-beach deposit (G.R. Lee and Park, 2018). The single age from the sand deposits was 108±18 ka (WALIS LUM ID #464) (Table 3; G.R. Lee and Park, 2018, 2019a). Based on Eq. (9), we arrive at a RSL estimate of 5.8±0.9 m (Table 3; WALIS RSL ID #4032).

4.4.2 Haenam area

Subsite Haenam-Ijin-ri is located 4-8 m above MSL and is comprised of sandy and clayey silt beds with granules and pebbles (D.Y. Yang et al., 2016). The gravel is a mixture of rounded to sub-angular clasts. These deposits were originally interpreted as marine sediments within a marine terrace, based on chemical analysis of the clay minerals (D.Y. Yang et al., 2016). However, no distinctive sedimentological or geomorphologic characteristics of the deposit suggest a marine origin. On the contrary, the poorly sorted sandy/clayey silt deposits with dispersed gravels look like overwash deposits in a backshore or alluvial setting behind the shoreline (e.g., J.Y. Lee et al., 2013; K.H. Choi et al., 2014). Four OSL ages acquired from the deposits at 4.95, 5.41, 6.49, and 7.51 m above MSL in the outcrop were dated as 152±11 (not included in WALIS), 128±9, 128±10, and 121±10 ka, respectively (D.Y. Yang et al., 2016). The three MIS 5e ages from the fine-grained silt sediments of 128±9 ka (WALIS LUM ID #467), 128±10 ka (WALIS LUM ID #466), and 121±10 ka (WALIS LUM ID #465) (Table 3; D.Y. Yang et al., 2016) are included in the WALIS database and interpreted as terrestrial limiting records of 4.3±1.3, 5.3±1.3, and 6.4±1.3 m, respectively (Table 3).

4.4.3 Buan area

The Buan area on the west coast of the Korean Peninsula (Fig. 7) has two localities, Buan-Daehang-ri and Buan-Mapo-ri, located 11 m and 9 m above MSL, respectively (G.R. Lee and Park, 2018). At the two localities, the outcrop exposes a mixture of silt, sand, and well-rounded pebbles and cobbles, approximately 2 m thick (G.R. Lee and Park, 2018). These deposits were originally interpreted as alluvial or marine sediments (G.R. Lee and Park, 2018) with little distinctive sedimentological or geomorphologic evidence for a marine origin. The two OSL ages from the sandy sediments were 112±24 ka (WALIS LUM ID #468) and 130±20 ka (WALIS LUM ID #469) (Table 3; G.R. Lee and Park, 2018, 2019a), which are interpreted as terrestrial limiting records.

4.5 Paleo-intertidal and nearshore deposits of the west coast

4.5.1 Seocheon area

Core DSR-C03 was collected onshore of a modern high-tide beach near Seocheon on the west coast of the Korean Peninsula (Fig. 7; Chang et al., 2017). MIS 5e deposits occur lower than about 1.5 m below MSL (Fig. 9). These occurrences of LIG deposits at approximately -1.5 m in elevation are the shallowest LIG deposits found in the core sediments acquired on the west coast of the Korean Peninsula. Four depositional units labeled as Units A, B1, B2, and C, in ascending stratigraphic order, were identified based on sediment texture and structures (Figs. 9, 10).

4.5.1.1 Unit A

The lowermost Unit A is mud-rich with sandy beds showing an overall coarsening-upward trend and attains a thickness of up to 12.5 m in core DSR-C03 (Fig. 9). This unit is comprised of lower muddy beds and upper more sandy beds (Fig. 9), both of which contain tidal couplets of mud and sand (Fig. 10D, E). The lower muddy beds are characterized by intense bioturbation,

no shell or rare shell fragments, and lenticular to wavy tidal bedding, while the upper more sandy beds show moderate

450 bioturbation, few shell fragments, and flaser to wavy and lenticular tidal bedding. Considering the presence of mud-sand tidal bedding and muddy nature of the sediments with no shell or rare shell fragments, the lower muddy beds are interpreted as being deposited in upper mud-flat or salt-marsh environments (e.g., Klein, 1985; Dalrymple et al., 1992; Dalrymple, 2010). The upper moderately bioturbated more sandy beds are suggestive of being deposited in an intertidal mixed-flat environment. The uppermost part of Unit A resembles the pre-Holocene semi-consolidated oxidized beds commonly occurring on top of

455 tidal-flat sequences throughout the west coast of Korea (e.g., Y.H. Kim et al., 1999; Lim et al. 2004; H.H. Yoon et al., 2021). The two OSL ages of 116±10 ka and 108±8 ka suggest that the tidal deposit formed during the MIS 5 period (Table 3; Fig. 9; e.g., Chang et al. 2014; Baek et al. 2017; H.H. Yoon et al., 2021).
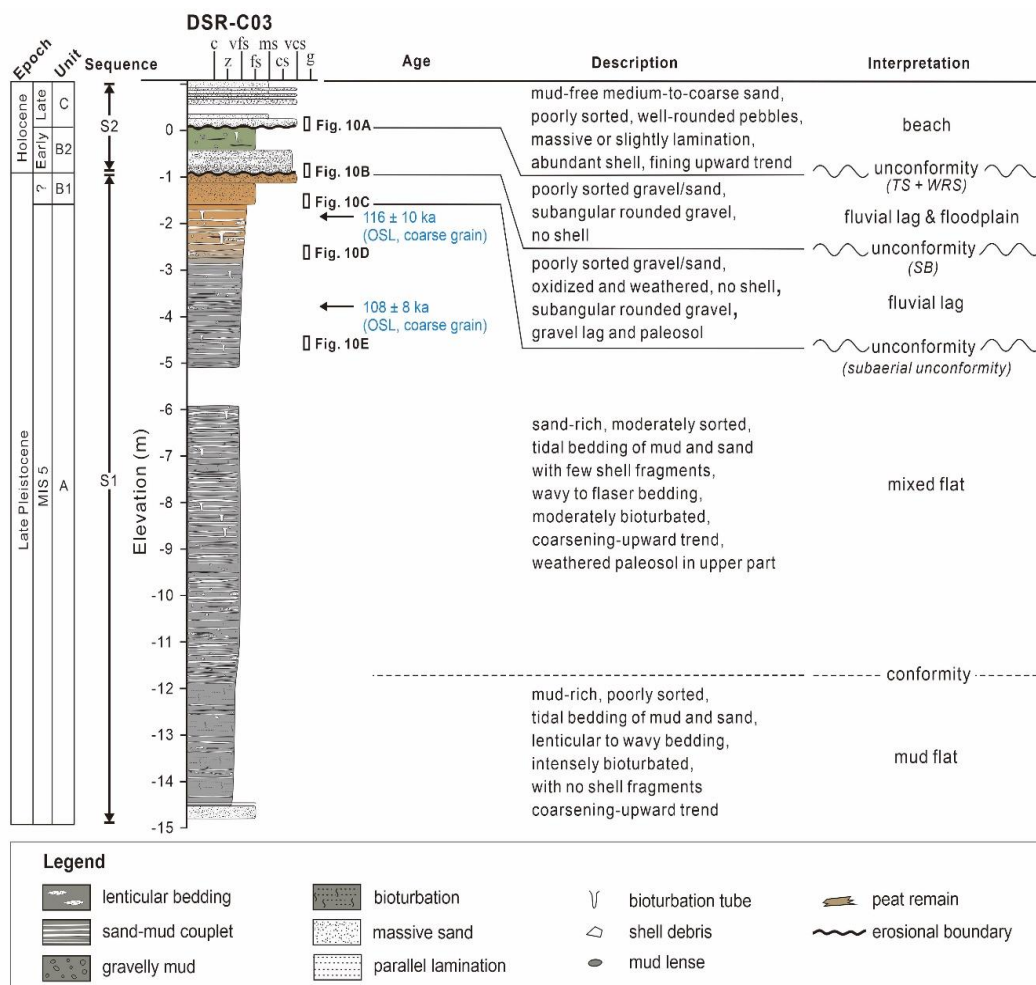
460 **Figure 9: Schematic columnar section of core DSR-C03 including lithology and OSL ages (cf. Chang et al., 2017). Two ages in bleu indicate LIG ages (WALIS LUM ID #470 and #471 in Table 3). For the location of the core, see Fig. 7. TS: Transgressive Surface, WRS: Wave Ravinement Surface, SB: Sequence Boundary**
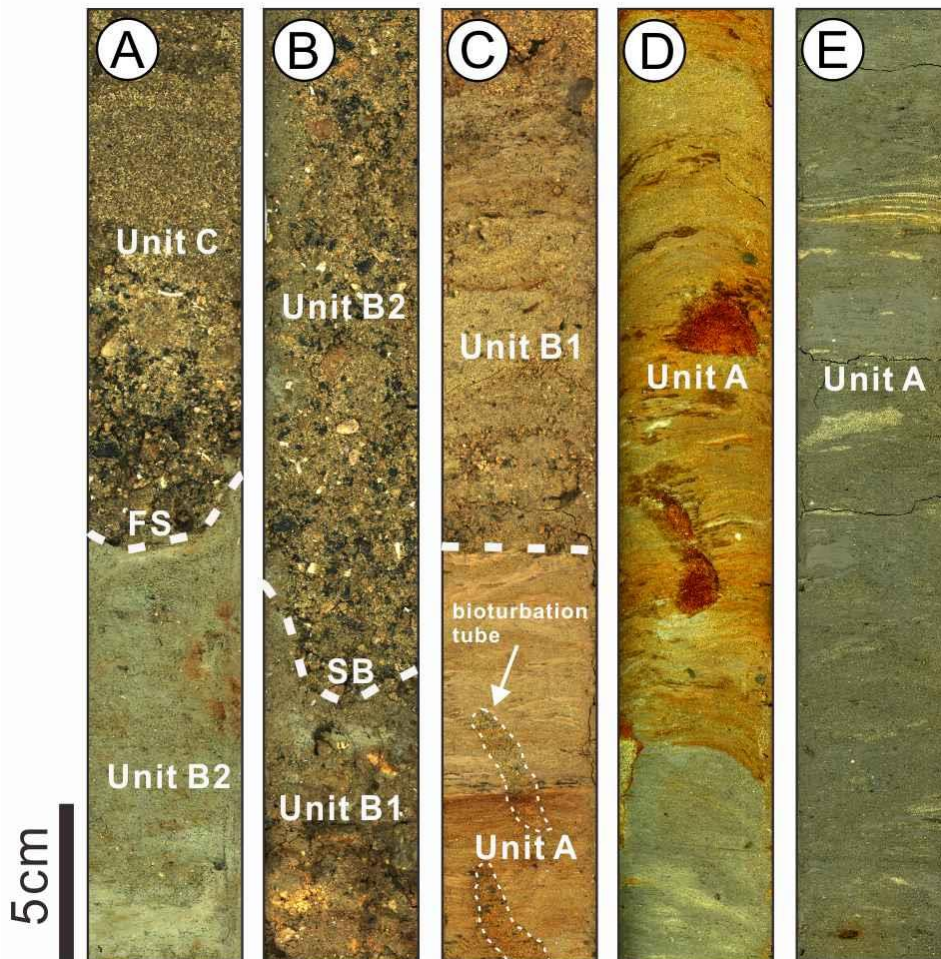
465 **Figure 10: Selected photographs of sediments in core DSR-C03 in Fig. 9. (a) Massive mud-free sand beds with laminated sand, pebble, shell-rich layers (Unit C). (b) Muddy coarse-grained sediments with weakly oxidized poorly sorted gravel and sand (Unit B2). (c) Completely oxidized poorly sorted gravel and sand without muddy sediments (Unit B1). (d, e) Moderately bioturbated, laminated, sandy mud and muddy sand with moderate flaser, wavy to lenticular bedding and rhythmic lamination (Unit A). The oxidized upper part of Unit A is reddish while the lower part has a gray color. TRS: Transgressive Ravinement Surface, SB:**
470 **Sequence Boundary**

Two OSL ages were obtained from Unit A in core DSR-C03. The one MIS 5e OSL age obtained from a coarse quartz sand bed was 116±10 ka (WALIS LUM ID #470) at -3.01 m below MSL. Another MIS 5e/5c OSL age of 108±8 ka (WALIS LUM ID #471) was obtained at a core depth of -4.95 m below MSL (Table 3; Chang et al., 2017). The shallowest occurrence of LIG

475 deposits in Unit A represents the highest among marine limiting records of LIG RSL.

OSL-dated clastic tidal-flat deposits were used as paleo RSL markers, identified based on sediment texture and sedimentary structures, and interpreted as tidal environments (e.g., Mauz and Bungenstock, 2007). Although some interpretations are of

salt-marsh deposits or intertidal mixed-flat deposits, no microfaunal work has been conducted on the deposits to confirm their marsh and mixed-flat interpretations and thus tightly constrained relationship with paleo-sea levels as is normally done in other

480   salt-marsh or intertidal based RSL studies (e.g., Shennan et al., 2015). Thus the tidal-flat data points are treated as marine limiting records because their relationship to past tidal-datums is not constrained by biological indicators.

4.5.1.2 Unit B

Unit B is approximately 2 m thick and is separated from the underlying Unit A by a distinct erosional boundary (Figs. 9, 10C). This unit can be further subdivided into two subunits: the lower unit B1 consists of completely oxidized gravel and sand devoid

485   of muddy sediments and the upper unit B2 contains muddy sediments with less oxidized gravel and sand sediments compared to unit B1. The sediments are composed of poorly sorted gravel and coarse sand (Fig. 10B, C). These units contain neither shells, foraminifers nor any other marine indicators. Muddy deposits of Unit B2 are commonly associated with coarser sand layers and contain wood fragments, fine peat, and rootlets. The erosional unconformities at the base of Units B1 and B2 and the presence of oxidized sediments point to an extended period of subaerial exposure. The contact is interpreted as a sequence

490   boundary (Figs. 9, 10B). The coarse-grained sediments without a muddy matrix probably originated from gravel bars or channel lag deposits in a fluvial environment (e.g., K. Choi and Kim 2006; Chang et al. 2014; Baek et al. 2017).

4.5.1.3 Unit C

Unit C is characterized by an upper massive sand bed and a lower crudely stratified sand bed showing a fining-upward trend (Fig. 9). The sand beds are mud-free and contain shell-rich beds (Fig. 10A). The upper sand beds are a few decimeters thick,

495   structureless, and comprised of very poorly sorted medium to coarse yellowish sand. The lower crudely stratified sand beds contain granules and pebbles (Fig. 10A). These characteristics suggest a swash deposit in the beach face. Unit C rests on a sharp erosional boundary separating it from the underlying sand/mud deposits of Unit B2 (Figs. 9, 10A). The erosional boundary is interpreted as a transgressive ravinement surface, formed by landward shoreface retreat and wave action in a shoreline during transgression and thus these deposits likely post-date the last glacial maximum (Fig. 9).

500   **4.5.2 Younggwang area**

Two cores were obtained on a modern tidal flat at Baeksu and Baeksu-Duuri near Younggwang (Fig. 7; Chang et al., 2014; Baek et al., 2017). Core 11YG-C4 at Baeksu has approximately 18 m of LIG deposits between -38 and -20 m below MSL (Fig. 11). The LIG deposit is characterized by tidal rhythmites, sand-mud couplets, and a lower stiff tidal mud with fine peats, rootlets, and wood fragments (Chang et al., 2014). The characteristics of the presumed LIG deposit are indicative of deposition

505   within a tidal mud-flat and salt-marsh environment (Chang et al., 2014). The twelve OSL LIG ages from 4-11 μm quartz grains were 110.0±6.6 ka (WALIS LUM ID #472) at -20.8 m in elevation, 133.9±7.6 ka (WALIS LUM ID #473) at -22.1, 124.0±7.8 ka (WALIS LUM ID #474) at -23.9 m, 138.8±7.8 ka (WALIS LUM ID #475) at -25.2 m, 128.7±7.9 ka (WALIS LUM ID #476) at -26.8 m, 124.7±7.6 ka (WALIS LUM ID #477) at -28.3 m, 118.8±7.0 ka (WALIS LUM ID #478) at -29.8 m,

112.2±6.8 ka (WALIS LUM ID #479) at -31.3 m, 113.4±7.1 ka (WALIS LUM ID #480) at -32.8 m, 118.2±7.4 ka (WALIS LUM ID #481) at -34.3 m, 112.6±6.9 ka (WALIS LUM ID #482) at -35.8 m, and 113.1±7.3 ka (WALIS LUM ID #483) at -37.3 m in elevation (Table 3; Chang et al. 2014). These occurrences suggest marine limiting records of LIG RSL.

In core 11YG-C01 from Baeksu-Duuri, LIG deposits occur between -31 and -19 m below MSL (Fig. 11). The LIG deposits attain a thickness up to approximately 12 m in the core and are characterized by tidal rhythmites, sand-mud couplets, a massive sand bed, and a fully bioturbated bed representative of tidal mud-flat and salt-marsh environments (Baek et al., 2017). It also contains shell beds, a lower stiff silt, mottled mud, partly deformed mud, fine peats, and wood fragments (Baek et al., 2017). The three OSL LIG ages from the fine quartz were 107.7±6.7 ka (WALIS LUM ID #484) at -15.5 m in elevation, 122.1±7.2 ka (WALIS LUM ID #485) at -26.0, and 126.2±8.1 ka (WALIS LUM ID #486) at -27.3 m in elevation (Table 3; Baek et al., 2017), suggesting marine limiting records of LIG RSL.

4.5.3 Gochang area

Core 15DH-C03 in the Gochang area was obtained from the modern nearshore environment and contains LIG deposits between -32 and -39 m below MSL (Figs. 7, 8; H.H. Yoon et al., 2021). The LIG deposit attains a thickness of up to ~7 m in the core, which is characterized by muddy beds containing no shell or rare shell fragments (Fig. 11; H.H. Yoon et al., 2021). Sediments in the lower part of the core mainly consist of laminated mud beds with some mud-sand couplets or lenticular bedding. The sediments contain a few bioturbated beds. Sediments in the upper part of the core are largely mottled, intensely bioturbated, and composed dominantly of silty mud. The sediments contain some dark-gray organic-rich beds with wood fragments. Based on the presence of mud-sand couplets and lenticular bedding, the lower laminated mud beds are interpreted as being deposited in an upper mudflat environment (H.H. Yoon et al., 2021). The upper bioturbated mud with some organic material suggests deposition within a tidal salt-marsh environment (H.H. Yoon et al., 2021). The presence of tidal mud-sand couplets and ages between MIS 5e and 5d suggests that the tidal deposit formed during or shortly after the LIG period (e.g., Chang et al. 2014; Baek et al. 2017). The three OSL MIS 5 ages from 4-11 μm quartz grains were 107.5±7.6 ka (WALIS LUM ID #487) at -35.2 m below MSL, 107.6±7.3 ka (WALIS LUM ID #488) at -37.4 m below MSL, and 113.3±7.2 ka (WALIS LUM ID #489) at -38.2 m below MSL (Table 3; H.H. Yoon et al., 2021), suggesting marine limiting records of LIG RSL.

4.5.4 Jindo area

Core H-C11 was obtained from the region offshore and south of Jindo (Fig. 7). A LIG age was obtained from sediments at an elevation of -48.5 m (S.H. Hong et al., 2019). This massive sandy shell bed was interpreted as a shelf deposit, based on the presence of swaley cross strata and abundant oyster fragments (Fig. 11; S.H. Hong et al., 2019). The single OSL LIG age from 4-11 μm quartz grains was 124.4±10.0 ka (WALIS LUM ID #490) at an elevation of -48.5 m (Table 3; S.H. Hong et al., 2019). This deposit provides a marine limiting record of LIG RSL.
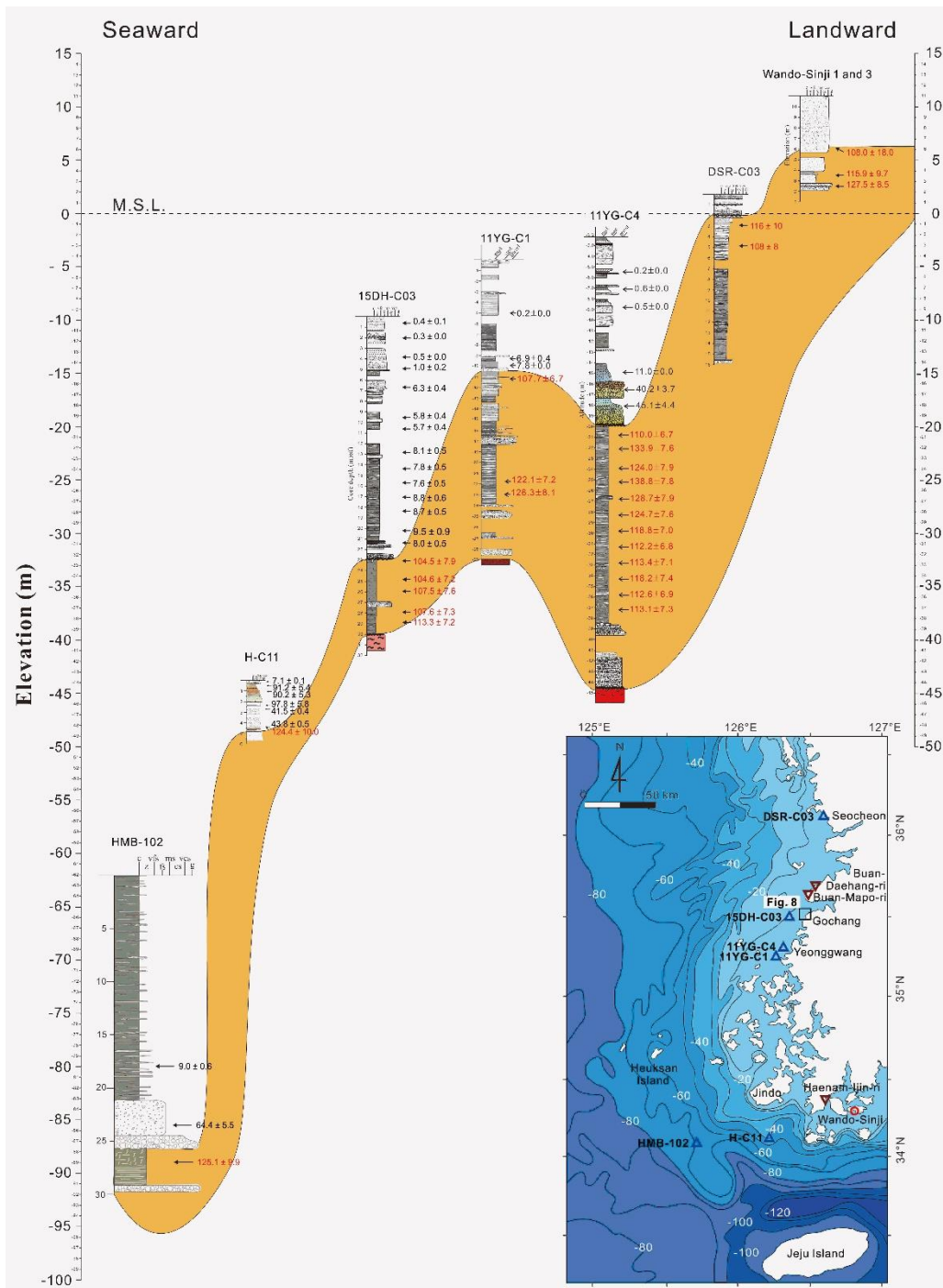
Figure 11: Onshore sections (Wando-Sinji 1 and 3) and tidal-to-nearshore cores (DSR-C03 to HMB-102) along the west coast of Korea plotted with respect to elevation of the remnant LIG deposits. Orange shading highlights the correlation of LIG deposits across the 6 coastal cores and Wando outcrop sections. Ages in red indicate LIG ages (WALIS LUM ID #470 to #491 in Table 3). For location, see Fig. 7.

4.5.5 Heuksan Mud Belt area

Core HMB-102 of the Heuksan Mud Belt was obtained from the modern offshore environment (Fig. 7). One LIG age in the core was obtained at -84 m from a tidal deposit of laminated silt and clay and mottled mud (Fig. 11; Chang and Ha, 2015). The single OSL LIG age from 4-11 μm quartz grains was 125.1±9.9 ka (WALIS LUM ID #491) at an elevation of -84 m (Table 3; J. C. Kim et al., 2019). This deposit represents a marine limiting record of LIG RSL.

5. Related sea-level topics

5.1 Uplift

The seismic stratigraphy and geology of the Gangneung and Donghae areas of the east coast of South Korea were summarized by Kwon et al. (2009) and Ryang et al. (2014). Intense compressional deformation during the early Pliocene, accompanied by the formation of reverse faults, strike-slip faults, and anticlinal folds, occurred mainly along the western margin of the submerged South Korea Plateau of the East Sea (Fig. 12; Ryang et al., 2007; Kwon et al., 2009). This deformation resulted in partial uplift and erosion of Late Pliocene and Early Quaternary deposits (Fig. 13). The lower boundaries of the post-Miocene stratigraphic units represent a progressive onlap termination against the apices of anticlinal folding (Fig. 13; Kwon, 2005; Kwon et al., 2009).

The southern region of the east coast may have also experienced considerable vertical displacement and deformation reflecting tectonic uplift during the Late Pleistocene along regional faults such as the Hupo, Yangsan, and Ulsan faults (J.H. Choi et al., 2003, 2009; S.J. Choi et al., 2008). All of the differential uplift is interpreted to be the result of backarc closing under a compressional regime since the early Pliocene (5 Ma) (S.H. Yoon and Chough, 1995; Chough et al., 2000). Although not all of the cross-coast faults along the east coast have been documented, local vertical movement and deformation probably caused marine terraces to experience uplift at different rates (Figs. 14, 15). This suggests their elevations largely reflect differential tectonic uplift (e.g., J.H. Choi et al., 2003, 2009; S.J. Choi et al., 2008, 2016).

We estimated rates of tectonic uplift of the marine terraces along the east coast of the Korean Peninsula using Eq. (12) and the five shoreline angle elevations listed in Table 2.

$$\text{Uplift Rates (m/ka)} = \frac{(Elevation\ of\ SA - MHHW - Assumed\ LIG\ Sea\ Level)}{Age} \qquad (12)$$

where SA represents the elevation of the shoreline angles and MHHW represents the mean higher high water at the subsites. The ages of the deposits associated with each of the SA can be found in Table 4. From Eq. 12, we arrive at uplift rates of 0.189 ± 0.031 m/ka, 0.195 ± 0.037 m/ka, 0.251 ± 0.024 m/ka, 0.172 ± 0.024 m/ka, and 0.198 ± 0.024 m/ka for Gangneung-Anin, Donghae-Eodal-dong, Pohang-Yonghan-2, Pohang-Masan-ri, and Gyeongju-Jinri, respectively, if assuming a LIG RSL of +3 m for the Korean Peninsula, and 0.166 ± 0.030 m/ka, 0.171 ± 0.035 m/ka, 0.228 ± 0.022 m/ka, 0.146 ± 0.023 m/ka, 0.174 ± 0.022 m/ka, respectively, in the case of a +6 m LIG RSL for the Korean Peninsula (Table 4). The error ranges were calculated

575 based on both the range of SA elevations and the age uncertainty (Table 4). The uplift rates for the northern and southern regions of the east coast are sufficiently different as to suggest differential uplift across the region (Table 4; Fig. 2).

Table 4. Uplift rates based on the elevation of the shoreline angles listed in Table 2 and LIG RSLs of +3 m and +6 m, respectively, along the east coast of the Korean Peninsula.

Site	Subsite	Sample latitude (°)	Sample longitude (°)	Shoreline angle elevation (m)	± Error range (ka)	Mean higher high water (MHHW) (m)	WALIS LUM ID	Age (ka)	± Age uncertainty (ka)	In case of LIG RSL +3 m		In case of LIG RSL +6 m	
										Uplift rate (m/ka)	± Error of uplift rate (m/ka)	Uplift rate (m/ka)	± Error of uplift rate (m/ka)
Gangneung	Anin	37.7401	128.9716	27.5	2.5	0.09	436	129.0	8.0	0.189	0.031	0.166	0.030
Donghae	Eodal-dong	37.5657	129.1181	28	2	0.07	438	128.0	14.0	0.195	0.037	0.171	0.035
Pohang	Yonghan-2	36.1085	129.4230	35	0	0.09	450	127.0	12.0	0.251	0.024	0.228	0.022
Pohang	Masan-ri	36.0152	129.4826	23.5	1.5	0.09	451	119.0	8.0	0.172	0.024	0.146	0.023
Gyeongju	Jinri	35.6827	129.4686	28	1	0.05	457	126.0	10.0	0.198	0.024	0.174	0.022

580

5.2 Subsidence

The currently-dated LIG sites along the west coast of Korea are all subject to potential subsidence rather than tectonic uplift. LIG deposits are found at lower elevations with greater water depth but these likely reflect deposition in progressively deeper waters during either the preceding rise in sea levels (MIS 6) or the fall in sea levels following the LIG highstand (Figs 1, 11).
585 LIG deposits appear to be better preserved basinward (Fig. 15). This preservation may be a result of erosion of the higher LIG deposits during subsequent sea-level falls (e.g., MIS 5d – MIS 2). Preservation of the deeper LIG deposits may have also been aided by their tectonic setting with increasing subsidence basinward. However, constraining the magnitude of Quaternary subsidence independent of the LIG elevation has yet to be attempted. Regional tectonic studies independent of the LIG shoreline elevation are needed to determine subsidence rates and correct LIG sea levels from its influence.

590
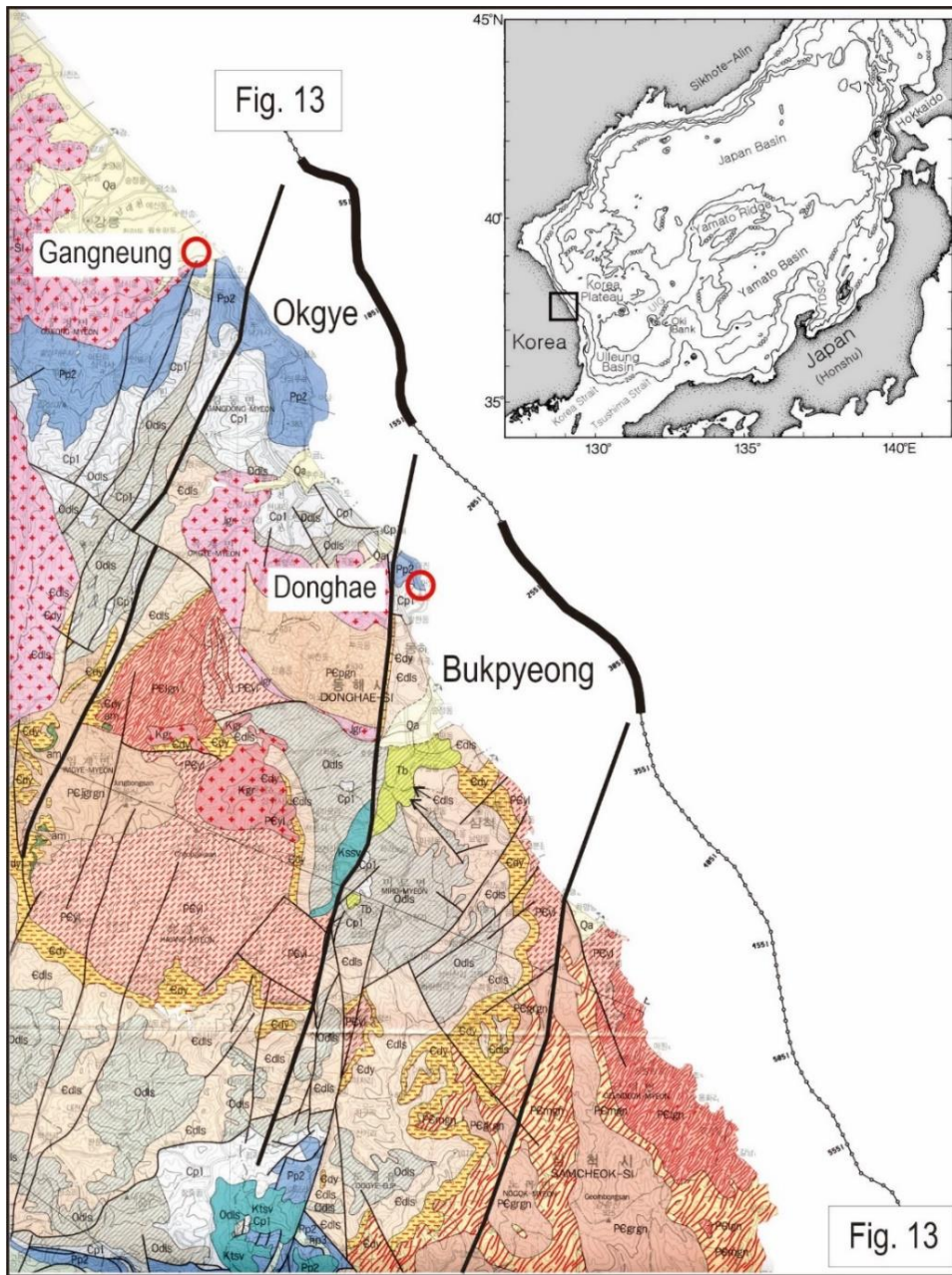
Figure 12: Geological map (1:250,000) and seismic track line around the Gangneung and Donghae areas (modified after J.C. Kim et al., 2005; Ryang et al., 2007, 2014). The multichannel seismic profile with interpretation is shown in Fig. 12. Red circles indicate the locations of LIG ages in Fig. 2. Solid lines indicate major strike-slip or thrust faults. Two thicker parts of the track line represent the interval of thick sedimentary bodies in the seismic profile of Fig. 12. Inset shows this figure area (solid rectangle) and adjacent land and sea (Chough et al., 2000). Legend codes of the geologic map (J.C. Kim et al., 2005): Qa, Quaternary Alluvium; Tb, Tertiary Bukpyeong Group; Kgr, Cretaceous granite; Kssv, Ktsv, Cretaceous Kyeongsang Supergroup; Jgr, Jurassic granite; Pp2, Permian Middle Pyeongan Group; Cp1, Carboniferous Lower Pyeongan Group; Odls, Ordovician Upper Great Limestone Group; ∈dls, Cambrian Lower Great Limestone Group; ∈dy, Cambrian Yangduk Group; P∈jgrgn, P∈grgn, P∈lgn, P∈mgn, P∈yl, Precambrian Metamorphic Complex.

Figure 13: Seismic section obtained parallel to the coastline and its stratigraphic interpretation (modified after Kwon, 2005; Ryang et al., 2007, 2014). For the location of the seismic track line, see Fig. 12.

Shoreline Angle Elevations along the East Coast
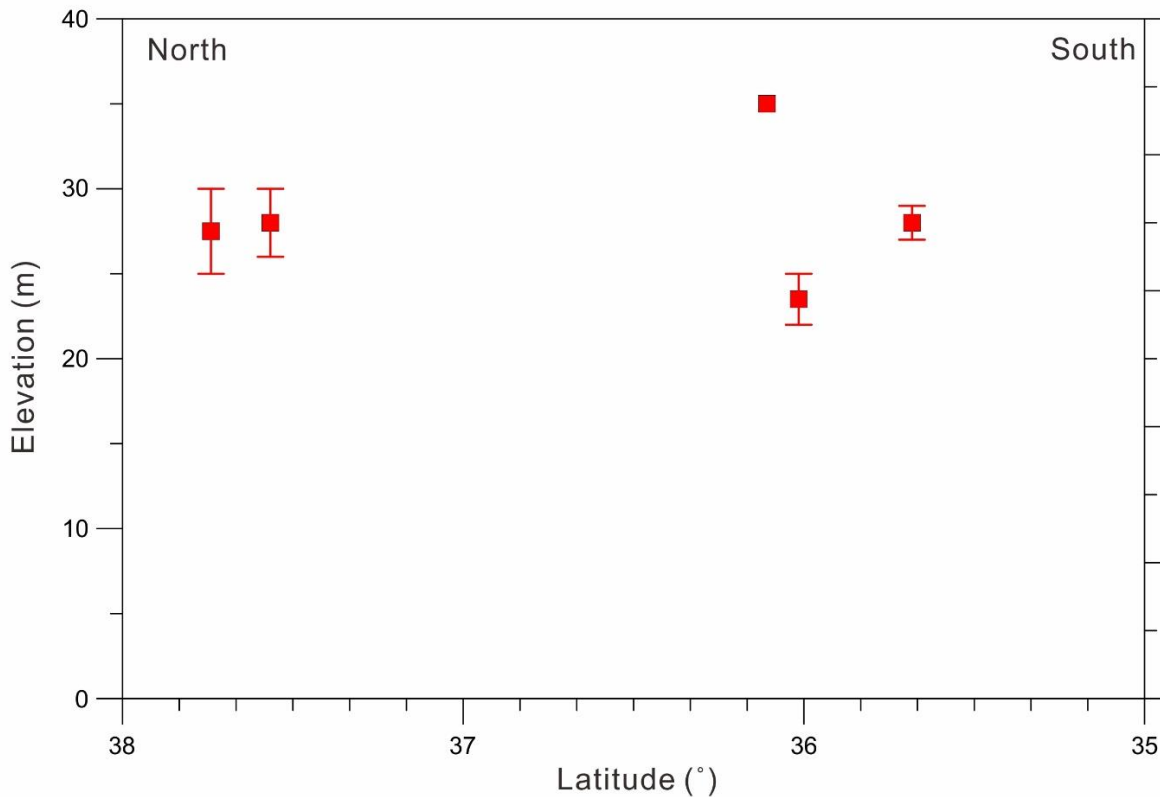
Figure 14: LIG relative sea level of the shoreline angles with respect to latitude along the east coast of Korea. See Table 2 to more details.

605
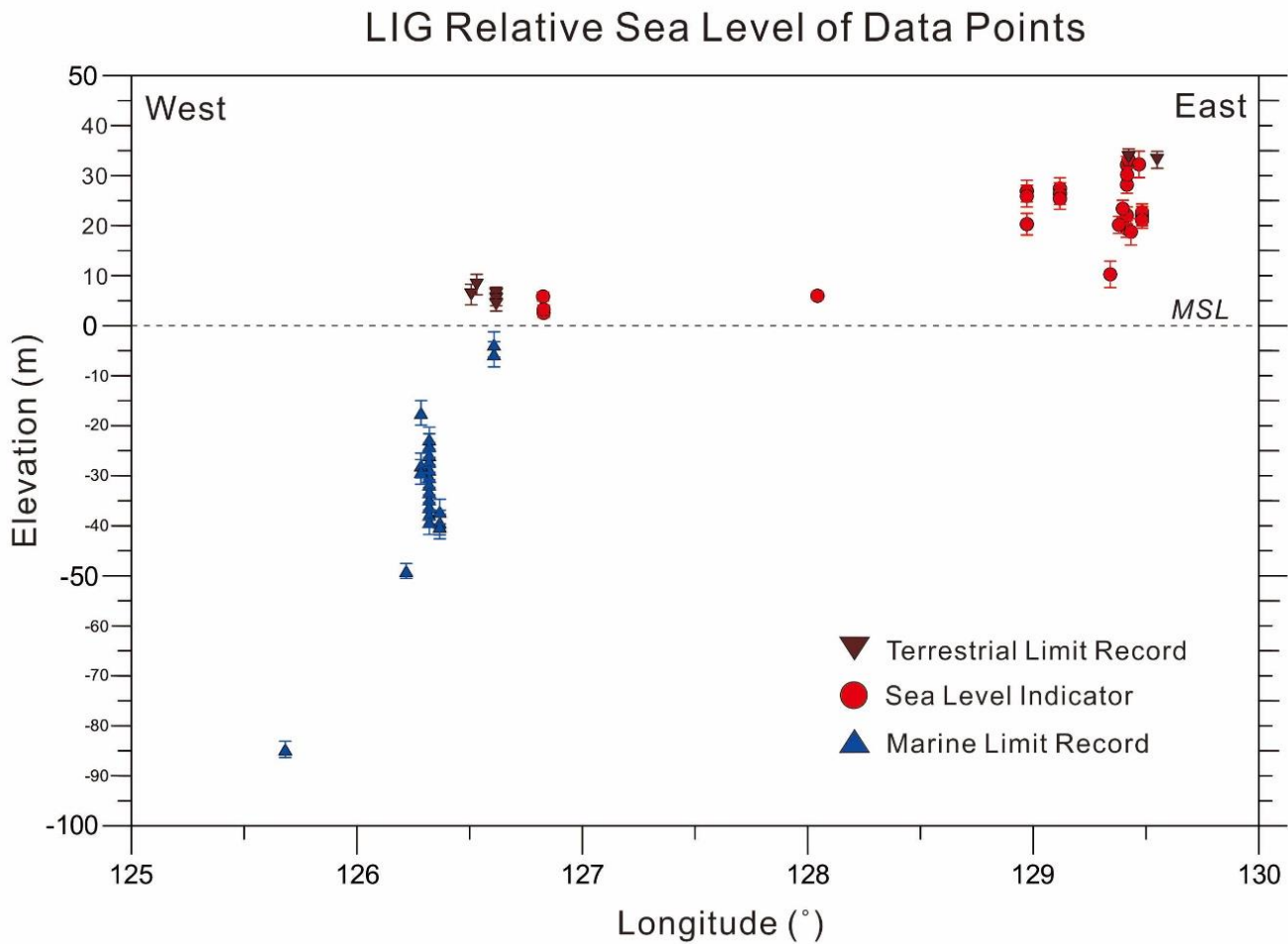
Figure 15. LIG relative sea levels with respect to longitude across the Korean Peninsula. See Table 3 for more details.

5.3 LIG sea-level fluctuations

Most ages of the LIG features in the Korean Peninsula were obtained via OSL. The error range of the OSL method is too large for the confident identification of fine-scale oscillations in LIG sea levels. The relatively few occurrences of LIG deposits also limit tests for LIG sea-level oscillations along the Korean Peninsula.

5.4 Earlier highstands

Four IRSL ages ranging from 185 to 221 ka were obtained from paleo-beach deposits on marine terraces of earlier highstands at 59 to 63 m above MSL in the Gangneung area of the east Korean coast (Fig. 2; S.C. Hong, 2014). In this area, three ages between 211 and 253 ka were also dated by cosmogenic [10]Be dating of paleo-beach deposits on marine terraces at 6l to 66 m above MSL (S.Y. Lee et al., 2015). More work is needed to better document earlier sea-level highstands on the Korean Peninsula.

5.5 Holocene sea-level indicators

Representative Holocene sea-level curves are well constrained along the west coast of the Korean Peninsula based on intertidal features and other sea-level indicators (Bloom and Park, 1985; Y.H. Kim et al., 1999; Chang and Choi, 2001; Chough et al., 2004; E. Lee and Chang, 2015). However, the curves are limited by the absence of preserved tidal deposits as well as sparse ages on tidal-flat sea-level indicators from 6500 to 3000 yrs ago, dissimilar to those of the Yangtze delta plain in China (Chough et al., 2004; S.J. Choi, 2018; H.H. Yoon et al., 2021). K.H. Choi (2009) suggested the possibility of a sea-level highstand around 6000 yrs ago based on OSL-dated onland sand dune deposition, but he also noted the absence of age data covering the period between 5000 and 3500 yrs ago in his study. Another suggestion is the possibility of a higher-than-present mid-Holocene highstand based on palynological data on land (Hwang and Yoon, 2011; Song et al., 2018), but these deposits lack a proper sedimentological description and stratigraphic framework. Further work remains to be done in reconstructing mid-Holocene sea levels along the Korean Peninsula.

5.6 Uncertainty and data quality

As all the summarized age data are based on OSL, with the exception of a single paleomagnetic age, the ages of the LIG shoreline features in the Korean Peninsula are only accurate and precise enough to establish a MIS 5 age, not necessarily which interstadial the features were deposited during. The age uncertainty is partially controlled by the mineral dated, either quartz or K-feldspar, as well as assumptions related to complete bleaching of the grains and their water content through time. The average error of the 42 OSL measurements using quartz minerals is 9.7 ka, and that of the 10 OSL measurements on K-feldspar minerals is 20.7 ka. The large age uncertainty in dating K-feldspar minerals is more than double that of dating quartz. This range of 9.7 to 20.7 ka is thought to be far too large to determine exactly within MIS 5 the deposits formed. However, based on their stratigraphic occurrences as the highest deposits from the region, we interpret most of the OSL-dated deposits as MIS 5e in age. Although the basement massif in the west coast of Korea has been assumed to be stable or undergoing minor subsidence during the Quaternary (Chough et al., 2010), the uncertainty in LIG sea levels is probably not free of additional error from possible subsidence or uplift around the Korean Peninsula.

6 Concluding remarks

The LIG shoreline is well developed as a marine terrace along the east coast of the Korean Peninsula and MIS 5 deposits are prevalent within the onshore and nearshore west coast. The east coast contains prevalent beach deposits on many marine terraces along the peninsula. The east coast LIG deposits suggest RSLs between +9 and +32 m (Table 3; Fig. 15). However, the uplifted terraces upon which these ages were obtained are likely inflenced by faulting under a compressional regime as a result of backarc closing of the East Sea (Table 2; Fig. 14). As a result, tectonic uplift likely biases the elevation of the east coast LIG shorelines. On the contrary, LIG sea levels appear to be well constrained to between +3 and +6 m by marine limiting records, sea-level indicators, and terrestrial limiting records along the west coast of the Korean Peninsula (Table 3; Fig. 15);

the most stable side of the Peninsula, although minor subsidence of the western coast cannot be ruled out. Further work is needed to establish credible sea-level indicators within the onshore portions of the west coast of the Korean Peninsula.

7 Data availability

The Korean Peninsula Last Interglacial sea-level database is available open access, and updated as necessary, at the following link: https://doi.org/10.5281/zenodo.4974826. The files at this link were exported from the WALIS database interface on June 17, 2021. A description of each field in the database can be found at this link: https://doi.org/10.5281/zenodo.3961543 (Rovere et al., 2020) and is accessible and searchable here: https://walis-help.readthedocs.io/en/latest/. More information on the World Atlas of Last Interglacial Shorelines can be found here: https://warmcoasts.eu/world-atlas.html.

Author contributions

WHR read the papers for the data, compiled the data, and wrote the initial manuscript. ARS initiated this work and revised the manuscript and dataset. HHY wrote the section of core DSR-C03 and drew most of the modified and original figures in this paper. Further input and discussion on the data and manuscript were provided by SSC and GSK. All authors revised the final text and agree with its contents.

Acknowledgments

This research was supported by research funds of Jeonbuk National University in 2020 and the National Research Foundation of Korea (NRF) grant funded by the Korean government (MSIT) (NRF-2019R1F1A1057715). GSK was supported by the project of development of the integrated geophysical survey and real scale data processing technologies for 3D high-resolution imaging of the marine subsurface (21-3312-1) of KIGAM. We acknowledge that the core DSR-C03 kept in Marine Core Center of KIGAM was used. The data used in this study were compiled in WALIS, a sea-level database interface developed by the ERC Starting Grant "WARMCOASTS" (ERC-StG-802414), in collaboration with PALSEA (PAGES / INQUA) working group. The database structure was designed by A. Rovere, D. Ryan, T. Lorscheid, A. Dutton, P. Chutcharavan, D. Brill, N. Jankowski, D. Mueller, M. Bartz, E. Gowan, and K. Cohen.

References

Baek, Y. S., Lee, S. H., and Chang, T. S.: Last interglacial to Holocene sedimentation on intertidal to subtidal flats revealed by seismic and deep-core sediment analyses, southwest coast of Korea, Quaternary International, 459, 45-54, 2017.

Bradley, W. C., and Griggs, G. B.: Form, genesis, and deformation of central California wave-cut platforms, Geological Society of America Bulletin, 87, 433-449, 1976.

Bloom, A. L. and Park, Y. A.: Holocene sea-level history and tectonic movements, Republic of Korea, The Quaternary Research, 24, 77-84, 1985.

680 Chang, J. H. and Choi, J. Y.: Tidal-flat sequence controlled by Holocene sea-level rise in Gomso Bay, west coast of Korea, Estuarine, Coastal and Shelf Science, 52, 391-399, 2001.

Chang, T. S. and Ha, H. J.: The Heuksan mud belt on the tide-dominated shelf of Korea: a supply-driven depositional system? Geo-Marine Letters, 35, 447-460, 2015.

Chang, T. S., Kim, J. C., and Yi, S.: Discovery of Eemian marine deposits along the Baeksu tidal shore, southwest coast of
685 Korea, Quaternary International, 349, 409-418, 2014.

Chang, T. S., Hong, S. H., Chun, S. S., and Choi, J. H.: Age and morphodynamics of a sandy beach fronted by a macrotidal mud flat along the west coast of Korea: a lateral headland bypass model for beach-dune formation, Geo-Marine Letters, 37, 361-371, 2017.

Choi, J. H.: Luminescence ages of quaternary marine sediments on the eastern coast of Korea and their geomorphic
690 implications, Ph.D. thesis, Seoul National University, Republic of Korea, 137 pp., 2004.

Choi, J. H., Murray, A. S., Cheong, C. S., Hong, D. G., and Chang, H. W.: The resolution of stratigraphic inconsistency in the luminescence ages of marine terrace sediments from Korea, Quaternary Science Reviews, 22, 1201-1206, 2003.

Choi, J. H., Cheong, C. S., and Chang, H. W., 2004, Principles of quartz OSL (Optically Stimulated Luminescence) dating and its applications, Journal of the Geological Society of Korea, 40, 567-583, 2004 (in Korean with English abstract)

695 Choi, J. H., Kim, J. W., Murray, A. S., Hong, D. G., Chang, H. W., and Cheong, C. S.: OSL dating of marine terrace sediments on the southeastern coast of Korea with implications for Quaternary tectonics, Quaternary International, 199, 3-14, 2009.

Choi, K. and Kim, S. P.: Late Quaternary evolution of macrotidal Kimpo tidal flat, Kyonggi Bay, west coast of Korea, Marine Geology, 232, 17-34, 2006.

Choi, K. H.: Evolution of Coastal Dune System and Sea Level Change during Holocene in Korea, Ph.D. thesis, Seoul National
700 University, Republic of Korea, 192 pp., 2009. (in Korean with English abstract)

Choi, K. H., Chang, T. S., Choi, J. H., Kim, Y. M., and Lee, S. Y.: Burial storm deposits recorded at the coastal dunes, Dasari, Chungnam Province, Journal of the Geological Society of Korea, 50, 539-549, 2014. (in Korean with English abstract)

Choi, S. G.: The last interglacial sea levels estimated from the morphostratigraphic comparison of the Late Pleistocene fluvial terraces in the eastern coast of Korea, The Korean Journal of Quaternary Research, 7, 1-26, 1993. (in Korean with English
705 abstract)

Choi, S. G.: Last interglacial marine geomorphic surfaces between Gangneung to Muckho in mid-eastern coast of Korean Peninsula, Journal of the Korean Geomorphological Association, 2, 9-20, 1995a. (in Korean with English abstract)

Choi, S. G.: The comparison and chronology of the lower marine terraces in the mid-eastern coast of Korean Peninsula, Journal of the Korean Geographical Society, 30, 103-119, 1995b. (in Korean with English abstract)

710 Choi, S. G.: Chronological study of Late Pleistocene marine terraces around Pohang area, southeastern coast of Korea, Journal of the Korean Geomorphological Association, 3, 29-44, 1996. (in Korean with English abstract)

Choi, S. G.: Tectonic movement in the southwestern coast of the Korean Peninsula indicated by marine terraces of Soando Island, Journal of the Korean Geomorphological Association, 13, 1-10, 2006. (in Korean with English abstract)

Choi, S. G.: The estimation of the marine terrace of the Last interglacial culmination stage (MIS 5e) in the Sanhari of Ulsan coast, southeastern Korea, Journal of the Korean Geomorphological Association, 23, 47-59, 2016a. (in Korean with English abstract)

Choi, S. G.: The estimation of the marine terrace of the late warm period of the Last Interglacial in the Sajin coast of Yeongdeok, southeastern coast of Korea, Journal of the Association of Korean Geographers, 5, 281-287, 2016b. (in Korean with English abstract)

Choi, S. G. and Chang, H.: Correlation and chronology of the marine terraces and thalassostatic terraces in the Yeongdeok coast, south eastern Korean Peninsula, Journal of the Korean Geomorphological Association, 26, 81-96, 2019. (in Korean with English abstract)

Choi, S. G., Tamura, T., Miyauchi, T., and Tsukamoto, S.: The examination of the limitations of using the OSL dates derived from this study in the correlation of MIS 5 marine terraces distributed in the southeastern coast of the Korean Peninsula, Journal of the Korean Geomorphological Association, 25, 63-75, 2018. (in Korean with English abstract)

Choi, S. J.: Marine terrace of the Jinha-Ilgwang area, southeast Korea, Economic and Environmental Geology, 36, 233-242, 2003. (in Korean with English abstract)

Choi, S. J.: Marine terraces and Quaternary faults in the Homigot and the Guryongpo, SE Korea, Journal of the Petrological Society of Korea, 25, 231-240, 2016. (in Korean with English abstract)

Choi, S. J.: Review on the relative sea-level changes in the Yellow Sea during the Late Holocene, Economic and Environmental Geology, 51, 463-471, 2018. (in Korean with English abstract)

Choi, S. J.: Review on marine terraces of the East Sea coast, South Korea: Gangreung – Busan, Economic and Environmental Geology, 52, 409-425, 2019. (in Korean with English abstract)

Choi, S. J., Merritts, D. J., and Ota, Y.: Elevations and ages of marine terraces and late Quaternary rock uplift in southeastern Korea, Journal of Geophysical Research: Solid Earth, 113, 1-15, 2008.

Chough, S. K.: Geology and Sedimentary of the Korean Peninsula, London, Elsevier, 1-363, 2013.

Chough, S. K., Lee, H. J., and Yoon, S. H.: Marine Geology of Korean Seas, Elsevier, Amsterdam, 1-313, 2000.

Chough, S. K., Lee, H. J., Chun, S. S., and Shinn, Y. J.: Depositional processes of late Quaternary sediments in the Yellow Sea: a review: Geosciences Journal, 8, 211-264, 2004.

Chun, S. S., Hwang, I. G., Ryang, W. H., Chang, T. S., Kim, J. G., and Yoon, H. H.: Western Pacific Sedimentology Meeting (WPSM) Field Trip Guide Book, Sedimentology of Holocene Tidal Flats (open coast & archipelago) and Cretaceous Nonmarine (strike-slip) Basin: Gwangju, Korean Sedimentology Research Group (KSRG), 1-117, 2018.

Creveling, J. R., Mitrovica, J. X., Clark, P. U., Waelbroeck, C., and Pico, T.: Predicted bounds on peak global mean sea level during marine isotope stages 5a and 5c, Quaternary Science Reviews, 193-208, 2017.

745   Cummings, D. I., Dalrymple, R. W., Choi, K., and Jin, J. H.: The Tide-dominated Han River Delta, Korea, Elsevier, Amsterdam, 1-376, 2016.

Dalrymple, R.W.: Tidal depositional systems, in: Facies Models 4, edited by: James, N.P. and Dalrymple, R.W., St. John's, Geological Association of Canada, 201-231, 2010.

Dalrymple, R. W., Zaitlin, B. A., and Boyd, R.: Estuarine facies models: conceptual basis and stratigraphic implications, Journal of Sedimentary Research, 62, 1130-1146, 1992.

750

Dutton, A. and Lambeck, K.: Ice volume and sea level during the last interglacial, Science, 337, 216-219, 2012.

Hong, S. C.: Constraining the Depositional Age of Marine Terrace Sediments along the Eastern Coast of Korea using Optical Dating, Ph.D. thesis, Seoul National University, Republic of Korea, 160 pp., 2014. (in Korean with English abstract)

Hong, S. C.: Principle and geomorphological application of rock surface luminescence dating, Journal of the Korean Geomorphological Association, 23, 127-136, 2016. (in Korean with English abstract)

755

Hong, S. C., Choi, J. H., Yeo, E. Y., and Kim, J. W.: Principles of K-Feldspar IRSL (InfraRed stimulated luminescence) dating and its applications, Journal of the Geological Society of Korea, 49, 305-324, 2013 (in Korean with English abstract)

Hong, S. H., Chang, T. S., Lee, G. S., Kim, J. C., Choi, J., and Yoo, D. G.: Late Pleistocene-Holocene sedimentary facies and evolution of the Jeju Strait shelf, southwest Korea, Quaternary International, 519, 156-169, 2019.

760   Hwang, S. I. and Yoon, S. O.: The characteristics of sedimentary facies and the geomorphological development of marine terraces in Kumgok area, Youngdeok county, east coast of Korea, Journal of the Korean Geomorphological Association, 3, 99-114, 1996. (in Korean with English abstract)

Hwang, S. I. and Yoon, S. O.: Holocene climatic characteristics in Korean Peninsula with the special reference to sea level changes, Journal of the Korean Geomorphological Association, 18, 235-246, 2011. (in Korean with English abstract)

765   Hwang, S. I. and Yoon, S. O.: The geomorphological development of marine terraces UHS (upper higher surface) and HHS (high higher surface) around Yeondae-san, Gampo-Eup, southeastern coast of Korea, Journal of the Korean Geomorphological Association, 27, 13-28, 2020. (in Korean with English abstract)

Hwang, S. I., Shin, J. Y, and Yoon, S. O.: Marine terrace and its implications to paleoenvironment during the Quaternary at Suje-ri – Suryum-ri of the east coast of Gyeongju, SE Korea, Journal of the Korean Geomorphological Association, 19,

770   97-108, 2012. (in Korean with English abstract)

Ingle, J. C. Jr.: Subsidence of the Japan Sea: stratigraphic evidence from ODP sites and onshore sections, Proceedings of the Ocean Drilling Program: Scientific Results 127/128 (part 2), College Station, TX, 1197-1218, 1992.

Inoue, D., Sasai, T., Yanagida, M., Choi, W. H., and Chang, C. J.: Stratigraphy of the marine terrace along the east coast in Korea by means of the loess-paleosol sequence and Japanese tephra, in: Abstract of the 2002 Autumn Conference of the

775   Geological Society of Korea, 24-26 October 2002, 81, 2002.

Jin, J. H., Chough, S. K., and Ryang, W. H.: Sequence aggradation and systems tracts partitioning in the mid-eastern Yellow Sea: roles of glacio-eustasy, subsidence and tidal dynamics, Marine Geology, 184, 249-271, 2002.

Klein, G. D.: Intertidal flats and intertidal sand bodies, Coastal Sedimentary Environments, Springer, 187-224, 1985.

Kim, Jeong C., Ko, H. J., Lee, S. R., Lee, C. B., Choi, S. J., and Park, K. W.: 1:250,000 Geological Report of the Gangneung-
780   Sokcho Sheets, Daejeon, Korea Institute of Geoscience and Mineral Resources, 76 pp., 2001. (in Korean with English
    abstract)

Kim, Jin C., Chang, T. S., and Yi, S.: OSL chronology of the Huksan Mud Belt, south-eastern Yellow Sea, and its
    paleoenvironmental implications, Quaternary International, 503, 170-177, 2019.

Kim, J. W., Chang, H. W., Choi, J. H., Choi, K. H., and Byun, J. M.: The morphological characteristics and geochronological
785   ages of coastal terraces of Heunghae region in northern Pohang City, Korea, Journal of the Korean Geomorphological
    Association, 12, 103-116, 2005a. (in Korean with English abstract)

Kim, J. W., Chang, H. W., Choi, K. H., and Lee, J.: Geomorphic and Geochronologic Survey of Coastal Terraces on the East
    Coast of Korean Peninsula, Korea Hydro and Nuclear Power Co., Res. Rep. E03NJ07, unpublished, 1-196, 2005b. (in
    Korean)

790 Kim, J. W., Chang, H. W., Choi, J. H., Choi, K. H., and Byun, J. M.: Landform characteristics of coastal terraces and optically
    stimulated luminescence dating on the terrace deposits in Yangnam and Yangbuk area of the Gyeongju City, South Korea,
    Journal of the Korean Geomorphological Association, 14, 1-14, 2007a. (in Korean with English abstract)

Kim, J. W., Chang, H. W., Choi, J. H., Choi, K. H., and Byun, J. M.: Optically stimulated luminescence dating on the marine
    terrace deposits of Hujeong-Jukbyeon region in Uljin, Korea, Journal of the Korean Geomorphological Association, 14,
795   15-27, 2007b. (in Korean with English abstract)

Kim, S. W.: A study on the terraces along the southeastern coast (Bang-eojin–Pohang) of the Korean Peninsula, Journal of
    Geological Society of Korea, 9, 89-121, 1973.

Kim, Y. H., Lee, H. J., Chun, S. S., Han, S. J., and Chough, S. K.: Holocene transgressive stratigraphy of a macrotidal flat in
    the southeastern Yellow Sea: Gomso Bay, Korea, Journal of Sedimentary Research, 69, 328-337, 1999.

800 Kopp, R. E., Simons, F. J., Mitrovica, J. X., Maloof, A. C., Oppenheimer, M.: Probabilistic assessment of sea level during the
    last interglacial stage, Nature, 462, 863-867, 2009.

Korea Hydrographic and Oceanographic Agency (KHOA), Ocean Data in Grid Framework,
    www.khoa.go.kr/oceangrid/gis/category/reference/distribution.do, last access: 16 June 2021. (in Korean)

Kwon, Y. K.: Sequence Stratigraphy of the Taebaek Group (Cambrian-Ordovician), Mideast Korea and Seismic Stratigraphy
805   of the Western South Korea Plateau, East Sea, Ph.D. thesis, Seoul National University, Republic of Korea, 205 pp., 2005.

Kwon, Y. K., Yoon, S. H., and Chough, S. K.: Seismic stratigraphy of the western South Korea Plateau, East Sea: implications
    for tectonic history and sequence development during back-arc evolution, Geo-Marine Letters, 29, 181-189, 2009.

Lee, D. Y.: Stratigraphic research of the Quaternary deposits in the Korean Peninsula, The Korean Journal of Quaternary
    Research, 1, 3-20, 1987.

810 Lee, E. and Chang, T. S.: Holocene sea level changes in the eastern Yellow Sea: a brief review using proxy records and
    measurement data, Journal of the Korean Earth Science Society, 36, 520-532, 2015. (in Korean with English abstract)

Lee, G. R. and Park, C. S.: Properties of deposits and geomorphic formative ages on marine terraces in Gwangyang Bay, South Sea of Korea, Journal of the Korean Geographical Society, 3, 346-360, 2006. (in Korean with English abstract)

Lee, G. R. and Park, C. S.: Study on Development and Distributional Characteristics of Terrace in the West and South Coast of Korea, Kyungpook National University and Korea Institute of Geoscience and Mineral Resources, unpublished, 1-111, 2018. (in Korean with English abstract)

Lee, G. R. and Park, C. S.: Comparison of uplift rate in the southern coast of the Korean Peninsula, Journal of the Korean Geomorphological Association, 26, 55-67, 2019a. (in Korean with English abstract)

Lee, G. R. and Park, C. S.: Production of Uplift Rate Map in the East Coast using Studies on Marine Terraces, Kyungpook National University and Korea Institute of Geoscience and Mineral Resources, unpublished, 1-106, 2019b. (in Korean with English abstract)

Lee, G. R. and Park, C. S.: Uplift rate map and distribution of uplift rate in the east coast of the Korean Peninsula, Journal of the Korean Geomorphological Association, 27, 47-60, 2020. (in Korean with English abstract)

Lee, J. Y., Kim, J. C., Lim, J., Kota, K., Hong, S. S., Moon, J. A., and Kim, Y. E.: Depositional environments and ages of coastal deposits in Gwanpo-ri, Geoje Island, Journal of the Geological Society of Korea, 49, 661-667, 2013. (in Korean with English abstract)

Lee, S. Y., Seong, Y. B., Kang, H. C., Choi, K. H., and Yu, B. Y.: Cosmogenic [10]Be and OSL dating of marine terraces along the central-east coast of Korea: spatio-temporal variations in uplift rates, The Open Geography Journal, 7, 28-39, 2015.

Li, C., Chen, G., Yao, M., and Wang, P.: The influences of suspended-load on the sedimentation in the coastal zones and continental shelves of China, Marine Geology, 96, 341-352, 1991.

Li, X. S., Zhao, Y. X., Feng, Z. B., Liu, C. G., Xie, Q. H., and Zhou, Q. J.: Quaternary seismic facies of the South Yellow Sea shelf: depositional processes influenced by sea-level change and tectonic controls, Geological Journal, 51, 77-95, 2016.

Lim, D. I., Jung, H.S., Kim, B.O., Choi, J.Y., and Kim, H.N.: A buried palaeosol and late Pleistocene unconformity in coastal deposits of the eastern Yellow Sea, East Asia, Quaternary International, 121, 109-118, 2004.

Marsset, T., Xia, D., Berne, S., Liu, Z., Bourillet, J. F., and Wang, K.: Stratigraphy and sedimentary environments during the Late Quaternary in the Eastern Bohai Sea (North China Platform), Marine Geology, 135, 97-114, 1996.

Mauz, B. and Bungenstock, F.: How to reconstruct trends of late Holocene relative sea level: A new approach using tidal flat clastic sediments and optical dating, Marine Geology, 237, 225-237, 2007.

Mauz, B., Vacchi, M., Green, A., Hoffmann, G., and Cooper, A.: Beachrock: a tool for reconstructing relative sea level in the far-field, Marine Geology, 362, 1-16, 2015.

Mayer, R. H. and Kriebel, D. L.: Wave runup on composite-slope and concave beaches, in: Proceedings of the 24th Coastal Engineering Conference, ASCE, 2325-2339, 1994.

Molnar, P. and Tapponnier, P.: Cenozoic tectonics of Asia - effects of a continental collision, Science, 189, 419-426, 1975.

Muhs, D. R., Kelsey, H. M., Miller, G. H., Kennedy, G. L., Whelan, J. F., and McInelly, G. W.: Age estimates and uplift rates
845   for late Pleistocene marine terraces: Southern Oregon portion of the Cascadia forearc, Journal of Geophysical Research, 95, 6685-6698, 1990.

Murray, A. S., and Wintle, A. G.: Luminescence dating of quartz using an improved single-aliquot regenerative-dose protocol, Radiation Measurements, 32, 57-73, 2000.

Nam, S. H., Lyu, S. J., Kim, Y. H., and Kim, K.: Correction of TOPEX/POSEIDON altimeter data for nonisostatic sea level
850   response to atmospheric pressure in the Japan/East Sea, Geophysical Research Letters, 31, L02304, 2004.

Nam, S. H., Park, J. H., and Park, J. J.: High-frequency variability: Basin-scale oscillations and internal waves/tides, in: Oceanography of the East Sea (Japan Sea), edited by: Chang, K.I., Zhang, C.I., Park, C., Kang, D.J., Ju, S.J., Lee, S.H., and Wimbush, M., Springer, Cham, 127-148, 2015.

National Geographic Information Institute: Korean Official Vertical Datum since 1964,
855   https://www.ngii.go.kr/eng/content.do?sq=110, last access: 16 June 2021.

Oh, G. H.: The geomorphic history of the southeastern coast of the Korean Peninsula, Geographical Review of Japan, 50, 689-699, 1977. (In Japanese with English abstract)

Oh, J. S.: Discussion on the characteristics and formation age of the reddish-yellow semi-consolidation deposits, west coast of Korea: comparison with the Ujeon coast deposits in Jeungdo, Journal of the Association of Korean Geographers, 7, 55-
860   68, 2018. (in Korean with English abstract)

Oh, I. S., and Lee, D. E.: Tides and tidal currents of the Yellow and East China Seas during the last 13000 years, Journal of the Korean Society of Oceanography, 33, 37-145, 1998.

Otvos, E.G.: Beach ridges – definitions and significance, Geomorphology, 32, 83-108, 2000.

Park, C. S., Kihm, Y. H., Nahm, W. H., and Lee, G. R.: Formative age of coastal terraces and uplift rate in the east coast of
865   South Korea, Journal of the Korean Geomorphological Association, 24, 43-55, 2017. (in Korean with English abstract)

Park, Y. A., Lim, D. I., Khim, B. K., Choi, J. Y., and Doh, S. J.: Stratigraphy and subaerial exposure of late Quaternary tidal deposits in Haenam Bay, Korea (south-eastern Yellow Sea): Estuarine, Coastal and Shelf Science, 47, 523-533, 1998.

Pugh, D. and Woodworth, P.: Sea-Level Science: Understanding Tides, Surges, Tsunamis and Mean Sea Level, Cambridge University Press, Cambridge, 1-395, 2014.

870 Ren, J., Tamaki, K., Li, S., and Junxia, Z.: Late Mesozoic and Cenozoic rifting and its dynamic setting in Eastern China and adjacent areas, Tectonophysics, 344, 175-205, 2002.

Rhodes, E. J.: Optically stimulated luminescence dating of sediments over the past 200,000 years, Annual Review of Earth and Planetary Sciences, 39, 461-488, 2011.

Rovere, A., Raymo, M. E., Vacchi, M., Lorscheid, T., Stocchi, P., Gomez-Pujol, L., Harris, D. L., Casella, E., O'Leary, M. J.,
875   and Hearty, P. J.: The analysis of Last Interglacial (MIS 5e) relative sea-level indicators: Reconstructing sea-level in a warmer world, Earth-Science Reviews, 159, 404-427, 2016.

Rovere, A., Ryan, D., Murray-Wallace, C., Simms, A., Vacchi, M., Dutton, A., Lorscheid, T., Chutcharavan, P., Brill, D., Batz, M., Jankowski, N., Mueller, D., Cohen, K., and Gowan, E.: Descriptions of database fields for the World Atlas of Last Interglacial Shorelines (WALIS), Zonodo, https://doi.org/10.5281/zenodo.3961543, last access: 16 June 2021.

880   Ryang, W. H., Kwon, Y. K., Jin, J. H., Kim, H. T., and Lee, C. W.: Geoacoustic velocity of basement and Tertiary successions of the Okgye and Bukpyeong coast, East Sea, Journal of the Korean Earth Sciences Society, 28, 367-373, 2007. (in Korean with English abstract)

Ryang, W. H., Kwon, Y. K., Kim, S. P., Kim, D. C., and Choi, J. H.: Geoacoustic model at the DH-1 long-core site in the Korean continental margin of the East Sea, Geosciences Journal, 18, 269-279 2014.

885   Ryang, W. H. and Simms, A. R.: Last interglacial sea-level proxies in the Korean Peninsula, https://doi.org/10.5281/zenodo.4974826. last access: 17 June 2021.

Schellart, W. P. and Lister, G. S.: The role of the East Asian active margin in widespread extensional and strike-slip deformation in East Asia, Journal of the Geological Society, 162, 959-972, 2005.

Shennan, I., Long, A. J., Horton, B. P.: Handbook of Sea-Level Research, American Geophysical Union & Wiley, Chichester,
890   1-581, 2015.

Shim, T. M.: Paleomagnetic Studies on the Coastal Terrace Deposits along the Youngil Bay, Eastern Coast of the Korean Peninsula, Ph.D. thesis, Yonsei University, Republic of Korea, 115 pp., 2006. (in Korean with English abstract)

Shin, J. Y. and Hong, S. C.: The formative processes and ages of paleo-coastal sediments in Daepo-dong Sacheon-si in the southern coast, South Korea: evaluation of the mode and rate of the late Quaternary tectonism (II), Journal of the Korean
895   Geomorphological Association, 25, 57-70, 2018. (in Korean with English abstract)

Shin, W. J., Yang, D. Y., and Kim, J. Y.: A study on the characteristics and burial age of sediment layers at Bukpyeong myeon, Haenam gun, Journal of the Korean Geomorphological Association, 23, 41-55, 2016. (in Korean with English abstract)

Shin, W. J., Lee, J. H., Byun, J., and Kim, J. Y.: The evidence for the high sea level of MIS 5e and the paleo-coastal sediments from Sinji-myen, Wando-gun, Jeollanam-do, Korea, Journal of the Korean Geomorphological Association, 26, 59-78,
900   2019. (in Korean with English abstract)

Shinn, Y. J., Chough, S. K., Kim, J. W., and Woo, J.: Development of depositional systems in the southeastern Yellow Sea during the postglacial transgression, Marine Geology, 239, 59-82, 2007.

Song, B., Yi, S., Yu, S. Y., Nahm, W. H., Lee, J. Y., Lim, J., Kim, J. C., Yang, Z., Han, M., and Jo, K. N.: Holocene relative sea-level changes inferred from multiple proxies on the west coast of South Korea, Palaeogeography, Palaeoclimatology,
905   Palaeoecology, 496, 268-281, 2018.

Tamaki, K., Suyehiro, K., Allan, J., Ingle J. C. Jr., and Pisciotto, K. A.: Tectonic synthesis and implications of Japan Sea ODP drilling, Proceedings of the Ocean Drilling Program: Scientific Results 127/128 (part 2), College Station, TX, 1333-1348, 1992.

Thompson, S. B. and Creveling, J. R.: A global database of Marine Isotope Stage 5a and 5c marine terraces and paleoshorelines
910   indicators, Earth System Science Data Discussions, https://doi.org/10.5194/essd-2021-14, last access: 16 June 2021.

US Army Corps of Engineers: Shore Protection Manual, Department of the Army, Waterways Experiment Station, Vicksburg, Chapter 2, 1-148, 1984.

Veeh, H.H.: Th^{230}/U^{238} and U^{234}/ U^{238} ages of Pleistocene high sea level stand, Journal of Geophysical Research, 71, 3379-3386, 1966.

915   Watson, M. P., Hayward, A. B., Parkinson, D. N., and Zhang, Z. M.: Plate Tectonic History, Basin Development and Petroleum Source Rock Deposition Onshore China, Marine and Petroleum Geology, 4, 205-225, 1987.

Yang, D. Y., Han, M., Kim, J. C., Lim, J., Yi, S, and Kim, J. Y. Characteristics of marine terrace sediments formed during the Marine Isotope Stage 5e in the west south coast of the Korean Peninsula, Economic and Environmental Geology, 49, 417-432, 2016. (in Korean with English abstract)

920   Yang, J. H. Morphogenetic succession and coastal climatic terrace associated with Quaternary climatic change, southern coast in Korean Peninsula, Journal of the Korean Geomorphological Association, 15, 93-110, 2008. (in Korean with English abstract)

Yang, J. H. Holocene sea level reflected from marine terrace in Geoje Island and its influences on coastal morphogenesis, Journal of the Korean Geomorphological Association, 18, 101-112, 2011. (in Korean with English abstract)

925   Yang, J. H., Kee, K. D., and Kim, Y. R.: Morpho-climatic milieu and morphogenetic succession of coastal terrace in Suncheon Bay, Journal of the Korean Geomorphological Association, 20, 57-74, 2013. (in Korean with English abstract)

Yoo, D. G., Lee, G. S., Kim, G. Y., Kang, N. K., Yi, B. Y., Kim, Y. J., Chun, J. H., and Kong, G. S.: Seismic stratigraphy and depositional history of late Quaternary deposits in a tide-dominated setting: An example from the eastern Yellow Sea, Marine and Petroleum Geology, 73, 212-227, 2016.

930   Yoon, H. H., Ryang, W. H., Chun, S. S., Simms, A. R., Kim, J. C., Chang, T. S., Yoo, D. G., and Hong, S. H.: Sensitive responses of coastal depositional system to the decreasing rates of Holocene sea-level rise in the macrotidal coast of Gochang, SW Korea, Journal of Sedimentary Research, in review, 2021.

Yoon, S. H. and Chough, S. K.: Regional strike-slip in the eastern continental margin of Korea and its tectonic implications for the evolution of Ulleung Basin, East Sea (Sea of Japan), Geological Society of America Bulletin, 107, 83-97, 1995.

935   Yoon, S. O., Hwang, S. I., and Jung, H. K.: A geomorphological development of marine terraces around Najung-ri and Daebo-ri at Gampo area, southeastern coast of Korea, Journal of the Korean Geomorphological Association, 6, 99-119, 1999. (in Korean with English abstract)

Yoon, S. O., Hwang, S. I., and Ban, H. K.: Geomorphic development of marine terraces at Jeongdongjin-Daejin area on the east coast, central part of Korean Peninsula, Journal of the Korean Geographical Society, 38, 156-172, 2003. (in Korean
940   with English abstract)

Yoon, S. O., Kwak, M., and Hwang, S. I.: Geomorphic development of marine terraces around the Kangdong area, Ulsan metropolitan city, southeastern coast of Korea, Journal of the Korean Geomorphological Association, 21, 147-163, 2014. (in Korean with English abstract)

Yoon, S. O., Park, C. S., and Hwang, S. I.: Geomorphic development of marine terraces in the Nampo area, Boryeong-si, Chungnam Province, Journal of the Korean Geomorphological Association, 22, 75-87, 2015. (in Korean with English abstract)